

AD-A247 001



A Study of Compressible Turbulence

by

David Nixon
Robert E. Childs
Laurence R. Keefe
Laura C. Rodman

Acc

A Study of Compressible Turbulence

by

David Nixon
Robert E. Childs
Laurence R. Keefe
Laura C. Redman

NEAR TR 443

February 1992



Accession For	
NTIS GRA&I	<input checked="" type="checkbox"/>
DTIC TAB	<input type="checkbox"/>
Unannounced	<input type="checkbox"/>
Justification	
By	
Distribution/	
Availability Codes	
Dist	Avail and/or Special
A-1	

Prepared for:
Air Force Office of Scientific Research
Bolling AFB, DC 20332

92-05581



Prepared by:
Nielsen Engineering & Research, Inc.
510 Clyde Avenue
Mountain View, CA 94043-2287
Telephone: (415)968-9457 • Facsimile: (415)968-1410

92 05581

REPORT DOCUMENTATION PAGE

Form Approved
OMB No. 0704-0188

Public reporting burden for this collection of information is estimated to average 1 hour per response, including the time for reviewing instructions, searching existing data sources, gathering and maintaining the data needed, and completing and reviewing the collection of information. Send comments regarding this burden estimate or any other aspect of this collection of information, including suggestions for reducing this burden, to Washington Headquarters Services, Directorate for Information Operations and Reports, 1215 Jefferson Davis Highway, Suite 1204, Arlington, VA 22202-4302, and to the Office of Management and Budget, Paperwork Reduction Project (0704-0188), Washington, DC 20503.

1. AGENCY USE ONLY (Leave blank)		2. REPORT DATE 31JAN92	3. REPORT TYPE AND DATES COVERED Final Report: 01JUN91 - 30NOV91	
4. TITLE AND SUBTITLE A Study of Compressible Turbulence			5. FUNDING NUMBERS F49620-91-C-0037	
6. AUTHOR(S) Nixon, D., Childs, R. E., Keefe, L. R., and Rodman, L. C.			3005/A1	
7. PERFORMING ORGANIZATION NAME(S) AND ADDRESS(ES) Nielsen Engineering & Research, Inc. 510 Clyde Avenue Mountain View, CA 94043-2287			8. PERFORMING ORGANIZATION REPORT NUMBER NEAR TR 443	
9. SPONSORING/MONITORING AGENCY NAME(S) AND ADDRESS(ES) AFOSR Building 410 Bolling AFB, DC 20332-6448			10. SPONSORING/MONITORING AGENCY REPORT NUMBER F49620-91-C 0037	
11. SUPPLEMENTARY NOTES				
12a. DISTRIBUTION/AVAILABILITY STATEMENT Approved for public release, distribution unlimited			12b. DISTRIBUTION CODE	
13. ABSTRACT (Maximum 200 words) This work involves theoretical analyses of turbulence in high speed flow and large eddy simulation results for the mixing layer. Analysis indicates that turbulence is dominated by streamwise vortices as the Mach number approaches infinity. A conceptual model based on swept vortices makes predictions about the sweep angle of these vortices from spanwise at low speeds to streamwise at high speeds, and about the reduced spreading rate at high speeds. Simulations of planar shear layers, started from random initial disturbances, validate these structural predictions. Some interesting characteristics about high speed turbulence have been identified. Shocks are generally rare and weak, even at a convective Mach number of 2.5, because the flow normal to the swept vortices is subcritical. The turbulence kinetic energy is dominated by streamwise fluctuations, while the other energy components are much smaller. The pressure-velocity correlations promote weak transfer of energy from the streamwise fluctuations to the other components of energy, and they strongly suppress the shear stress. These statistics are, in general, compatible with the swept vortex structure of turbulence at high Mach number.				
14. SUBJECT TERMS compressible turbulence, flow simulation mathematical models			15. NUMBER OF PAGES 37	
			16. PRICE CODE	
17. SECURITY CLASSIFICATION OF REPORT UNCLASSIFIED	18. SECURITY CLASSIFICATION OF THIS PAGE UNCLASSIFIED	19. SECURITY CLASSIFICATION OF ABSTRACT UNCLASSIFIED	20. LIMITATION OF ABSTRACT UL	

TABLE OF CONTENTS

INTRODUCTION	1
Objectives	2
Principal Results	3
THEORY	3
Inviscid Model	4
Simple Vortex Model	7
TURBULENCE SIMULATIONS	8
Navier-Stokes Solver - TMRC	9
Boundary Conditions	9
Code Validation	10
Domain and Grid	10
FLOW FIELDS	11
Temporally Evolving Flows	11
Spatially Evolving Flow	12
SIMULATION RESULTS	12
Shear Layer Growth	12
Dominant Structure	13
Shocklets	14
$M_c = 4$ Case	15
Turbulence Statistics	15
Pressure-Velocity Terms	18
The Role of Dissipation	20
Limitations	20
SUMMARY AND CONCLUSIONS	21
FUTURE WORK	22

A STUDY OF COMPRESSIBLE TURBULENCE

INTRODUCTION

One of the critical aspects of the aerodynamic design of high speed aircraft is the lack of understanding of (compressible) turbulence at these speeds. Turbulence can considerably affect the drag, heat transfer, and engine performance of the aircraft, and, consequently, it is imperative that the understanding of turbulence at hypersonic speeds be improved. It is proposed that as a first step the differences between compressible turbulence and the much better understood incompressible turbulence be better identified. In Phase I, these differences are investigated using data from numerical simulations of turbulence.

Among the many factors that influence "hypersonic turbulence" are compressibility, the appearance of fluctuating shock waves, real gas effects, catalytic wall effects, and rarefied gas effects. The influence of any of these factors on turbulence is unknown, and it would be a formidable task to include all of these in a single research effort. In this effort, only compressibility effects, including fluctuating shock waves, are considered. This factor is common to all hypersonic turbulence and must therefore be understood before substantial attention is devoted to the other factors.

There is a very considerable body of literature on turbulence phenomena at low (incompressible) speeds.¹ These investigations of low speed turbulence are either experimental,² or achieved by numerical simulation.³ The former does not give as much detail as the simulations, but does give information at realistic Reynolds numbers. Simulations are restricted to low Reynolds numbers because of the computer limitations and should only be used as a guide to the nature of phenomena at higher Reynolds numbers. At high speeds there have been experimental efforts^{5,6} to obtain data on hypersonic turbulence, but this has not progressed to the stage where underlying phenomena are understood. There is a general belief⁴ that compressibility effects in turbulence will occur only when the Mach number of turbulence fluctuations achieves magnitudes of 0.5 or higher. The freestream Mach (M_∞) number where this may occur depends on the type of flow; for a boundary layer, M_∞ is assumed to be about 5, whereas for mixing layers, it is about 1.5. Hypersonic flight vehicle configurations of interest may fly at Mach numbers from 5 to 25 depending on the mission, and since these are above the bounds where compressibility effects become important, it is critical that the nature of turbulence at these speeds be understood.

Some aspects of high speed turbulence are reasonably well understood. For example, a concentrated effort in compressible shear layers over the past several years has identified mechanisms which cause the onset of reduced turbulent mixing as the convective Mach number increases. In attached boundary layer flows, the Van Driest II theory which accounts for near wall heating performs quite well at freestream Mach numbers up to at least $M_\infty = 5.0$.

However, some turbulent flows at *very* high Mach numbers have been observed to behave differently than at merely high Mach numbers. For example, the laminar-to-turbulent transition in boundary layers can cover extended regions of flow, rather than being a brief intermediate stage at lower speeds. Furthermore, earlier studies¹¹ on a

boundary layer indicate that pressure fluctuations dominate the turbulence at a Mach number of 9.4, while vorticity fluctuations dominate low speed turbulence. Hence, there are indications that turbulence at very high Mach numbers may be fundamentally different than at low or moderate Mach numbers. The principal distinguishing characteristic of high Mach number flows is that the kinetic energy of the (free stream) flow is very much larger than the internal energy of the gas. At a Mach number of 10, for example, internal energy is only 5% of the kinetic energy. High speed flows are affected by strong near-wall heating resulting in reduced Reynolds numbers and expanded viscous regions, significant effects due to energy transferring between kinetic energy and gas compression, and shock waves which are often present.

Because compressibility effects appear there at relatively low Mach numbers, one of the most commonly studied problems^{7,8,9,10} in high speed turbulence is that of the free shear layer. Here two streams at different Mach numbers mix, with the dominant parameter being a convective Mach number, M_c , that is essentially a density weighted difference of the Mach numbers of the two streams. The general conclusion of these studies is that as M_c increases, mixing and, by implication, turbulence, decreases. These investigations of mixing layers were performed initially by means of experiment,⁸ but the major effects of compressibility have also been delineated by numerical simulation⁹ and analysis.¹⁰ All of the investigations are for $M_c < 2$, which represents the high supersonic regime.

The supersonic mixing layer is thus an accessible problem that displays compressibility effects on turbulence at relatively low speeds. It is easily computed and amenable to mathematical analysis, and thus an investigation of the differences between turbulence in compressible and incompressible layers should be straightforward. In particular, data from numerical simulations of compressible layers contain the effects of incipient shock formation, a feature that is generally believed to radically alter the structure of turbulence. For example, it is suggested in Ref 10 that just as a shock is about to form, the nominally two-dimensional mixing layer becomes three dimensional.

An important part of the proposed work is to investigate the role of vorticity in compressible turbulence. Much of incompressible turbulence phenomena can be described in terms of vorticity dynamics. As shown later, the vortical structure of turbulence at high Mach numbers is considerably different than at low speeds. Density and pressure fluctuations also become major factors at high speeds. In some respects, this conclusion is also corroborated in the mixing layer study of Ref. 10 which implies that at higher M_c vortical effects are reduced because of density changes.

This work is concerned with understanding the differences between incompressible and hypersonic turbulence using simulations of mixing layer flow at as high a convective Mach number as possible so that dominant compressibility effects can be clearly identified.

Objectives - Compressible mixing layers will be examined at as high a convective Mach number as possible in order to delineate compressibility effects on turbulence. The technical questions that will be addressed are as follows:

- (a) What are the differences between incompressible and hypersonic turbulence, especially the role of vorticity in the latter?
- (b) What is the role of shock waves or shocklets in hypersonic turbulence?

- (c) Is the standard description of turbulence based on velocity fluctuations suitable at hypersonic speeds or is there an alternative representation?

Because of the limited time and costs of a Phase I effort, it is expected that only a gross understanding of these topics can be obtained. This should provide sufficient information to identify areas for a more definitive study in Phase II.

Principal Results - This work involves theoretical analysis of turbulence in high speed flow and large eddy simulations of the planar mixing layer. Some of the key findings are as follows. One analysis indicates that, for turbulence to exist in the limit of the Mach number approaching infinity, turbulence must be dominated by streamwise vortices. An approximate model based on the idea of swept vortices at high mach number makes predictions about the sweep angle of these vortices from spanwise at low speeds to streamwise at high speeds, and about the reduced spreading rate at high speeds. Simulations of planar shear layers, started from random initial disturbances, validate the structural predictions of these theories. The simulations predict the dominance of spanwise vortical structures in the low speed layer, and that these structures are swept in the streamwise direction at high speeds. The normalized mixing rate is predicted to decrease significantly at high speeds. Hence, theory and simulation make consistent predictions about the structure of turbulence. There is, however, a significant element of ambiguity in the simulation results: calculations initiated with a deterministic disturbance derived from stability theory yielded a significantly different turbulent structure.

A preliminary analysis has been performed on the simulation results, and some interesting characteristics about the turbulence have been identified. For one, shocklets are generally rare and weak, even at a convective Mach number of $M_c = 2.5$. The turbulence kinetic energy is dominated by streamwise fluctuations, while the other two components of energy are smaller by roughly an order of magnitude. The pressure-velocity correlations promote weak transfer of energy from the streamwise fluctuations to the other components of energy, and they strongly suppress the shear stress. These findings are compatible with the unsteady pressure and vorticity fields observed in the simulations.

Hence, this rather brief Phase I effort has demonstrated theory and simulations which make consistent statements about high speed turbulence, and which agree with experimental observations. The statistical data analyzed so far indicate dramatic changes in the statistics between low and high speed flows and that this change may be caused by the altered vortex structure at high speeds.

THEORY

The analysis performed during this effort was intended to determine if broad statements can be made about the nature of turbulence as the Mach number becomes very large. The thermodynamics laws which lead to compressibility effects in turbulence are nonlinear and difficult to analyze. However, these laws can be approximated by more tractable forms over limited ranges to provide insights into phenomena which may occur in high speed turbulence.

Inviscid Model - It is frequently assumed that large scale turbulence can be represented by the Euler equations; although viscosity is necessary to initiate and sustain turbulence, its global features can be represented approximately in an inviscid model. The density, ρ , temperature, T , and pressure, p , in the steady Euler equations may be related to the velocity, q , and the entropy change, S , by

$$\frac{\rho}{\rho_r} = \left\{ 1 + \frac{(\gamma-1)}{2} M_r^2 (1 - q^2) \right\}^{\frac{1}{\gamma-1}} \exp(-S/R) \quad (1)$$

$$\frac{T}{T_r} = \left\{ 1 + \frac{(\gamma-1)}{2} M_r^2 (1 - q^2) \right\} \quad (2)$$

$$\frac{p}{p_r} = \left\{ 1 + \frac{(\gamma-1)}{2} M_r^2 (1 - q^2) \right\}^{\frac{\gamma}{\gamma-1}} \exp(-S/R) \quad (3)$$

where the subscript "r" denotes a reference value, perhaps in the region of turbulence production, γ is the ratio of specific heats, and R is the gas constant. The velocity q is normalized with respect to a reference value, q_r .

Let q' be a turbulent fluctuation about q_r , that is

$$q^2 = 1 + 2[u_r u' + v_r v' + w_r w'] + u'^2 + v'^2 + w'^2 \quad (4)$$

and let

$$\left. \begin{aligned} \rho/\rho_r &= 1 + \rho' \\ T/T_r &= 1 + T' \\ p/p_r &= 1 + p' \\ S/R &= S'/R \end{aligned} \right\} \quad (5)$$

If the reasonable assumption that the general fluctuating quantity f' satisfies

$$|f'| \ll 1 \quad (6)$$

is made, then, in order for ρ/ρ_r to be real

$$\frac{(\gamma-1)}{2} M_r^2 (q^2 - 1) < 1 \quad (7)$$

or

$$|u_r u' + v_r v' + w_r w' + (u'^2 + v'^2 + w'^2)/2| < 1/[(\gamma-1)M_r^2] \quad (8)$$

If Eq. (6) is applied, Eq. (8) becomes, to first approximation,

$$|u_r u' + v_r v' + w_r w'| < 1/[(\gamma-1)M_T^2] \quad (9)$$

If the flow is such that $u_r \gg v_r$ and w_r , then Eq. (9) indicates that

$$|u_r u'| \rightarrow 0 \text{ as } M_T \rightarrow \infty \quad (10)$$

which shows that the fluctuations become two-dimensional in the plane normal to the streamwise direction.

In a similar fashion, the relative magnitude of the nondimensional fluctuations in density, pressure, and temperature compared to the velocity can be determined. Expanding Eq. (1) in a series yields

$$\rho' = -S'/R - (q^2-1)M_T^2/2 + \underline{O} \{ [0.5(\gamma-1)M_T^2(1-q^2)]^2 \} \quad (11)$$

Then, because of Eq. (7), a first approximation to Eq. (11) is

$$\rho' = -S'/R - (q^2-1)M_T^2/2 \quad (12)$$

From Crocco's equation, entropy is related to vorticity Ω by

$$T \nabla(S/R) = (\bar{q} \times \bar{\Omega})(\gamma M_T^2) \quad (13)$$

in which \bar{q} and T are the velocity vector and temperature. By a rotational perturbation about an irrotational flow, it can be observed that to first approximation,

$$\nabla \times (S'/R) = (\bar{q}_r \times \bar{\Omega}')(\gamma M_T^2) \quad (14)$$

Using Eqs. (12) and (14), it can be shown that

$$\nabla \rho' - -\nabla(S'/R) - M_T^2 \nabla(q^2-1)/2 = -M_T^2 [\gamma \bar{q}_r \times \bar{\Omega}' + \nabla(q^2-1)/2] \quad (15)$$

Since ρ' is bounded, it can be inferred from Eq. (15) that as $M_T^2 \rightarrow \infty$,

$$\gamma \bar{q}_r \times \bar{\Omega}' + \nabla(q^2-1)/2 = 0 \quad (16)$$

If \bar{q}_r is dominated by u_r , then to first approximation, Eq. (16) gives

$$\left. \begin{aligned} u_r \partial u' / \partial x &= 0 \\ u_r \partial u' / \partial y &= \gamma u_r \Omega'_3 \\ u_r \partial u' / \partial z &= -\gamma u_r \Omega'_2 \end{aligned} \right\} \quad (17)$$

Consider now the vorticity transport equation

$$L(\bar{\Omega}) = \bar{\Omega}_r + (\bar{q} \cdot \nabla) \bar{\Omega} - (\bar{\Omega} \cdot \nabla) \bar{q} + \bar{\Omega} (\nabla \cdot \bar{q}) = -\nabla \times (\nabla p / \rho) / \gamma M_T^2 \quad (18)$$

The term on the right can be evaluated by combining Eqs. (1) and (3) to give

$$-\nabla \times (\nabla p / \rho) / \gamma M_T^2 = (\gamma - 1) \nabla(S/R) \times \nabla q^2 / 2 \quad (19)$$

or, by using Eq. (13),

$$-\nabla \times (\nabla p / \rho) / \gamma M_T^2 = (\gamma - 1) (\gamma M_T^2 / T) (\bar{q} \times \bar{\Omega}) \times \nabla q^2 / 2 \quad (20)$$

Using Eq. (20) in Eq. (18) and assuming that the normalized vorticity and velocity are bounded, then it may be seen that as $M_T^2 \rightarrow \infty$,

$$(\bar{q} \times \bar{\Omega}) \times \nabla q^2 \rightarrow 0 \quad (21)$$

If \bar{q} is dominated by u_r , then Eq. (21) gives the following possibilities:

$$\bar{\Omega} = 0 \quad (22a)$$

$$u_r \Omega_2 = u_r \Omega_3 = 0 \quad (22b)$$

$$u_r \Omega_2 \partial q^2 / \partial y - u_r \Omega_3 \partial q^2 / \partial z = 0 \quad (22c)$$

Equation (22a) states there is zero vorticity, and Eq. (22b) indicates that streamwise vortices dominate, that is, a Beltrami flow exists. If the problem is a geometrically two-dimensional flow, such that

$$|\partial q^2 / \partial z| \ll |\partial q^2 / \partial y| \quad (23)$$

then Eq. (22c) indicates that

$$u_r \Omega_2 \partial q^2 / \partial y = 0 \quad (24)$$

or

$$\Omega_2 = 0 \quad (25)$$

This indicates that vortices may either be streamwise or spanwise. If Eqs. (10) and (17) are combined, it may be seen that

$$\Omega_2 = \Omega_3 = 0 \quad (26)$$

leaving the only possibility that the vortices are predominantly in the streamwise direction.

Physically, the analysis indicates that once vorticity is introduced into the flow, its distribution is dominated by the entropy relation which restricts the type of vorticity allowed. To a first approximation, as the Mach number tends to infinity in a typical shear flow, the vortices are aligned with the mean streamwise direction, a direction which causes no entropy production.

Simple Vortex Model - From the above analysis, it appears that the vortical structures of turbulence will tend to be oriented in a streamwise direction as $M \rightarrow \infty$. As will be seen in the simulation results below, the structures at intermediate Mach numbers are highly swept towards the streamwise direction. It is possible, therefore, that the sweep angle of the structures increases with increasing Mach number, from zero sweep at incompressible speeds, to 90° as $M_c \rightarrow \infty$. If this is so, how does this structural change depend on the Mach number?

A simple theory for the sweep angle of the dominant structures can be constructed by postulating that the vortical structures are related to the spanwise ones in low speed shear layers, but that they respond only to the component of the flow which is normal to the vortices. For a vortex swept at an angle β with respect to the spanwise direction, the "effective" normal velocity difference across the layer and convective Mach number are

$$\Delta U_{\text{eff}} = \Delta U \cos(\beta) \quad (27a)$$

$$M_{c,\text{eff}} = M_c \cos(\beta) \quad (27b)$$

This model requires the empirically derived turbulent growth rate for two-dimensional structures

$$\sigma_{2D}(M_c) \quad (28)$$

Take σ_{2D} to be normalized by the incompressible growth rate, so that $\sigma_{2D}(0) = 1$. From two-dimensional simulations, σ_{2D} approaches zero as in Fig. 1 at about $M_c = 1$. For simplicity, this function is approximated as $\sigma_{2D} = 1 - M_c^2$. This approximation may be least valid as $M_c \rightarrow 1$, but this is largely irrelevant, it turns out, to the predictions made by the model. This analysis implicitly assumes that the growth rate of the turbulent layer is determined by the maximum possible growth rate over all sweep angles, which seems reasonable but is not proven.

Low speed shear layer experiments have demonstrated that the layer's growth rate depends upon $\Delta U / \bar{U}$ in which \bar{U} is the average of the velocities on either side of the shear layer. By the above postulate, this form applies for high speed layers with ΔU_{eff} replacing ΔU . \bar{U} is unchanged by the sweep angle. Hence, the velocity difference which provides the energy for the growth of the swept structures is reduced by a factor of $\cos(\beta)$, while the convective Mach number which suppresses growth is also reduced. The growth rate of the shear layer is that of the structures with no restraint on sweep angle, which is predicted to be

$$\sigma_{3D}(M_c, \beta) = \cos(\beta) \sigma_{2D}(M_c \cos(\beta)) \quad (29)$$

σ_{3D} is given in Fig. 2 for several angles β . At low Mach numbers the maximum growth rate is achieved with unswept structures, and $\sigma_{3D}(M_c, \beta)$ is unchanged from σ_{2D} . However, at $M_c = 0.6$ the swept structures have a more rapid growth rate than the unswept ones. As $M_c \rightarrow 1$ and $\sigma_{2D} \rightarrow 0$, the maximum growth rate is associated with increasingly swept structures. The envelope of the curves for σ_{3D} in Fig. 2 is similar in character to experimental measured dependence of spreading rate on the Mach number.

It is also possible to determine the sweep angle at which the growth rate is a maximum, as a function of convective Mach number, $\beta_{\sigma, \max}(M_c)$. This is plotted in Fig. 3. It shows $\beta_{\sigma, \max} = 0$ up to $M_c \sim 0.6$, at which point $\beta_{\sigma, \max}$ increases rapidly with M_c , and asymptotes to $\beta_{\sigma, \max} \rightarrow 90^\circ$ as $M_c \rightarrow \infty$. It is also worth noting that, to preserve zero net streamwise angular momentum, there must be vortices with opposite signs of sweep and streamwise vorticity.

It is worth reiterating that this is a very simple theory, in which "turbulence" is highly idealized and even then treated approximately. Small errors are to be expected; it is general consistency with experiment, simulation, and other theory that is sought.

Other theories for vortex sweeping at high convective Mach numbers also exist. The theory of Nixon and Keefe¹⁰ postulates that the vortex structure bifurcates and sweeps to avoid the formation of a shock wave. Typically, shock formation occurs at $M_c \sim 0.7$ in two-dimensional simulations, so that swept structures occur for $M_c > 0.7$. Hence, the Nixon - Keefe¹⁰ theory and the present one make comparable predictions about the onset of swept structures, but the underlying mechanisms appear to be very different. Shocks are related to, but in no sense directly linked to, the compressibility effects which suppress σ_{2D} with increasing M_c . These differences may become critical. If a good model is to be constructed for high speed turbulence, it is important for the model to be based on the correct underlying physics. Hence, it may be important in the near future to determine which of these and other theories gives the most accurate representation of the phenomena which control the turbulent structures.

Some of the strongest experimental support for the dominance of swept structures in high speed layers comes from the field of high speed jet aeroacoustics.¹² The structure of the dominant turbulent structures in the near field of a round jet, whether spanwise or swept vortices, can be deduced from the acoustic pattern. Axisymmetric acoustic modes are caused by axisymmetric structures which are spanwise in the initial jet shear layer, while helical modes indicate swept structures. Experiments reveal that axisymmetric modes dominate the near field up to jet Mach numbers of about $M_j \approx 1.2$, which corresponds to $M_c = 0.6$. Higher speed jets contain a variety of helical modes, depending upon M_j . While the axisymmetric shear layer is different than the plane one treated in the above theories, the underlying physical mechanisms are similar. Hence, there is strong experimental support for a transition to swept vortical structures at $M_c > 0.6 \sim 0.7$.

The above two theories described in Eqs. (1) - (26) and in (27) - (29) differ vastly in the assumptions employed and the depth of the analysis. However, both indicate that the vortices in a turbulent shear layer become aligned with the streamwise direction as the Mach number becomes very large.

TURBULENCE SIMULATIONS

At this point the focus of the work shifts to simulations of turbulence which will lend strong support to the above theoretical findings and will provide further insight into turbulence.

Navier-Stokes Solver - TMRC - The code employed to perform the large eddy simulations (LES) of the shear layer is called TMRC (for turbulence modeling research code). A brief description of the code and the details of the simulations are provided here.

The equations solved by TMRC are the full compressible Navier-Stokes equations for a perfect gas ($\gamma = 1.4$) and, if appropriate, equations for an eddy-viscosity or Reynolds-stress turbulence model. The Sutherland formula is used to determine the laminar viscosity. TMRC uses true fourth order central finite volume discretization for the convective terms and second order central differencing for the viscous fluxes. Artificial dissipation is employed in high-Reynolds number and in high Mach number flows to control "odd-even" oscillations that are not damped by viscosity, especially those which appear at shocks or during vortex stretching in turbulent flows. Both physical phenomena cause a rapid cascade of energy to high wave numbers and can cause the solution to diverge. A combination of linear fourth order and a nonlinear second/fourth order dissipation is used. In the nonlinear dissipation, second order viscous-like dissipation is employed, and the coefficient of dissipation depends on fourth derivatives. Fourth derivatives depend most strongly on the high wave number content of the solution; hence, the nonlinear dissipation behaves like a dynamical sub-grid-scale model, providing diffusive transport only if there is high wave number content in the solution. An explicit five stage Runge-Kutta procedure is used to integrate the equations in time.

The effects of sub-grid-scale (SGS) turbulence are modeled with a modified Smagorinsky eddy-viscosity model. This is generally to be regarded as a poor model which has several shortcomings for the present flow. However, the model directly affects only the smallest scale of turbulence, and it should not significantly alter the dominant features in the simulation results.

Boundary Conditions - The far-field boundary conditions, which must permit acoustic radiation and, in one case, vortex outflow, are treated with Thompson's¹³ non-reflecting boundary condition procedure. These boundary conditions are reasonable for acoustic radiation, but very poor for the outflow of vortices. Most simulations are of shear layers which are periodic in both directions in the plane of the shear layer, and evolving in time. The assumption of temporally evolving shear layers was employed to provide good resolution of turbulence, within the limited scope of the simulations that can be afforded during a Phase I effort. Given the assumption of periodicity, these boundaries are then treated exactly, and unsteady vorticity and acoustic signals pass through these boundaries properly.

It is important to insure that the assumption of periodicity does not compromise the accuracy of the simulation, and the issues of major concern are addressed here. One significant concern is that the periodic boundary conditions may impose significant constraints on the structure of turbulence which would render the simulated flow very different from the natural one. The computational domain used here has an aspect ratio in the plane of the shear layer of $(x_{\max} - x_{\min}) / (z_{\max} - z_{\min}) = 2$, where x is the streamwise direction, z is spanwise, and y is normal to the plane of the shear layer. A whole number of turbulent structures must fit into this domain because of the periodic boundary conditions, and, typically, a small number of structures exist, 1, 2, or 3. These conditions constrain the swept structures in the high speed shear layer to certain discrete sweep angles. The fewer the number of structures present, the larger the jumps between the permitted sweep angles.

A straightforward means of reducing this problem is to increase the size of the domain so that a large number of structures exist in the domain.

Simulations were performed on two sizes of computational domains. One was 50% larger than the other in all spatial directions, while the grid spacing and the initial shear layer thickness were unchanged. The principal difference between the results was that the statistics from the small-grid solution were less smooth. Qualitatively, the dominant features such as the structures and the growth rate were similar. This result suggests that these types of difficulties associated with periodicity are under control, though not necessarily negligible. All simulations reported herein were run on the larger domain.

Another issue with the periodic assumption is that of entropy and vorticity generation due to shock waves in the non-turbulent flow adjacent to the shear layer. Turbulent shear flows are clearly not periodic in the streamwise direction; entropy is generated if shocks are present, and turbulent mixing and dissipation generates entropy. However, computational studies contrasting spatially evolving and temporally evolving (streamwise periodic) low speed shear layers exhibit only very minor differences. A comparison of temporally and spatially evolving high speed layers was performed in support of this work. Because of the specific initial disturbances used to excite the layer, strong shocks formed. However, the vortical structures in the spatially and temporally evolving calculations were still very similar. Hence, the periodic assumption seems good enough to study many aspects of these flows. In fact, shock waves were seldom observed in the majority of the simulations which were started with random initial perturbations.

Code Validation - The code TMRC has been used in a very wide variety of flow simulations, and its ability to accurately solve the Navier-Stokes equations has been established. Some examples of previous calculations are given here. A pair of adjacent vortices interact to spin around one another, and this behavior can be described analytically in the limit of negligible viscous effects. Calculations of these flows were performed,¹⁴ and the computed solution converges to the analytical one as the grid is refined and the viscosity goes to zero. Fourth order accuracy was demonstrated. The code has been used to perform simulations of the axisymmetric mean flow and turbulence structure of a round jet. In the near field where the assumption of axisymmetric turbulence is reasonable, the predicted shock structure and mean velocity profiles agreed well with experimental measurements.¹⁴ The code has also been used to perform large eddy simulations of stratified turbulence,¹⁵ and simulations of a variety of impinging jet phenomena.^{16,17} In all cases the code has given results that agree well with analysis or experiment when limiting assumptions are satisfied. Hence, there is a high level of confidence in the solutions produced by TMRC.

TMRC has also been used to examine the enhanced turbulence in a jet impinging on the ground. An intriguing result of this study was the formation of fluctuating shock waves (or shocklets) due to the turbulent eddies in the impingement region. The simulations correctly predicted the enhancement of turbulence at specific frequencies due to fluid/acoustic feedback and unsteady shock formation.

Domain and Grid - The grids used for these simulations are Cartesian. For the spatially periodic simulations, the grid spacing in the x- and z-directions, which are in the plane of the shear layer, is uniform with $\Delta x / \delta_0 = \Delta z / \delta_0 = 0.5$, in which δ_0 is the initial shear layer thickness. Uniform grid spacing in the x- and z-directions was used to minimize any

bias in the formation of spanwise or streamwise turbulent structures. In the y-direction, normal to the plane of the shear layer, the grid is stretched, with a grid spacing of $\Delta y/\delta_0 = 0.2$ throughout the region of turbulence, stretching to $\Delta y/\delta_0 = 1.5$ at edges of the domain. The extent of the computational domain is

$$-18 < x/\delta_0 < 18, \quad -19.2 < y/\delta_0 < 19.2, \quad \text{and} \quad -8.5 < z/\delta_0 < 8.5$$

The grid used for the majority of simulations had $73 \times 85 \times 35$ points in the x-, y-, and z-directions. Statistics and structural data are obtained from the shear layers when they are typically about $\delta/\delta_0 = 4$, so that the dimensions of the domain are reasonably large relative to the shear layer thickness.

FLOW FIELDS

Free shear layers only were considered in this work. These are relatively simple flows, which are well studied, and which exhibit strong compressibility effects. The approach taken here is not limited to free shear flows; it can also be applied to temporally or spatially evolving boundary layers and other flows.

Temporally Evolving Flows - The principal characteristics which define each flow are the mean velocity and thermodynamic variables, and the initial disturbance field which will grow and become turbulence. The mean initial field consists of an approximately linear variation between the two end states of the velocity. In the one simulation which involved mean density variation, the density also varied linearly. The initial pressure was uniform in all cases.

Two types of initial disturbance fields were considered. In all but two simulations, the initial velocity field was computed as a smoothed random field. Initially the perturbation velocity field is specified randomly with a maximum magnitude of ΔU , the total velocity difference across the layer. The Cray random number generator RANF is used to obtain the random numbers. The initial disturbances were confined to a layer 20% thicker than the mean velocity profile, and they were scaled to be a maximum on the centerplane and to decay smoothly to zero at the edge of the region of disturbances.

$$\mathbf{u}' = \Delta U \text{RANF} F(|y-y_0|/(0.6\delta_0)) \quad (31)$$

The scaling function goes smoothly from $F(0) = 1$ to $F(1) = 0$. A different random number is used for each component, u' , v' , and w' , of the vector, \mathbf{u}' . This \mathbf{u}' field is then added to the mean velocity, and the complete velocity field is smoothed with second order smoothing, e.g.,

$$\mathbf{U}^{n+1} - \mathbf{U}^n = \epsilon \nabla^2 \mathbf{U}, \quad (32)$$

in which $()^n$ denotes the iteration and ϵ is a small number, until the velocity fluctuations are reduced considerably. The energy spectrum resulting from this smoothing process has a maximum at low wave numbers and decreases with increasing wave number, as occurs in physical turbulence. This velocity field is unlike low-level turbulence, and the first process to occur during the simulation is for the flow to relax to a physically plausible, although very random, disturbance field.

These initial conditions contain no organized structures, and any structures that appear in the solutions are formed as a result of the dynamical processes that govern turbulence.

The other type of initial disturbance was used in the spatially evolving calculation and a companion temporal simulation. It was a combination of three modes selected using the results of stability analyses. The fundamental two-dimensional mode for the initial shear layer, its first subharmonic, and a pair of oblique waves were combined for this case. This initial condition for the temporally evolving flow is the appropriate equivalent of the inflow conditions supplied to the spatially evolving flow described below.

Spatially Evolving Flow - The simulation of an $M_c = 1.$, spatially evolving shear layer was conducted on a $401 \times 76 \times 13$ (x,y,z) grid spanning a spatial domain of $0 < x/\delta_0 < 500$, $-15 < y/\delta_0 < 15$, and $-3 < z/\delta_0 < 3$. The value of $M_c = 1.$ was obtained by imposing $M_1=3.1$ and $M_2=1.1$, with constant density and pressure across the layer at the end of the splitter plate. The layer was excited at the plate trailing edge by spatial instability modes calculated from the stability code of Sandham and Reynolds¹⁸. To the most unstable 2D mode and its subharmonic were added a pair of oblique waves ($\beta = 78^\circ$) that had growth rates very near the 2D disturbance. For these waves the growth rate was about 50% of the maximum achievable at $\beta = 60^\circ$ for this convective Mach number. The simulation was run for times sufficient to allow initial disturbances at the splitter plate to pass completely out of the domain.

SIMULATION RESULTS

The principal results are from shear layers with a Mach number difference across the layers of $\Delta U/c = 0.4$ and $\Delta U/c = 5.0$ with a uniform mean density. The flows correspond to nominal convective Mach numbers of $M_c = 0.2$ and $M_c = 2.5$, respectively. In a third case the velocity difference $\Delta U = 8$. The density was varied to mimic the effects of constant stagnation temperature across the layer, with fast cold flow above the shear layer and hot stagnant fluid below it. This gives a nominal value of $M_c = 1.48$, assuming the convective Mach numbers are the same with respect to upper and lower freestreams. The final simulation to be discussed was at $\Delta U = 8$ and constant density to give $M_c = 4$.

Shear Layer Growth - The simulations were run until the shear layer thickness grows to $\delta - 6\delta_0$, typically. The growth is nonlinear while $\delta < 3\delta_0$, but is roughly linear for $4\delta_0 < \delta < 6\delta_0$. Figure 4 gives the shear layer thickness as a function of time for three different simulations. The linear growth rate suggests that the turbulence has reached some asymptotic state, beyond the effects of the initial conditions and before the structures become saturated in the computational domain. The results which are examined in detail and presented later are taken from this linear growth period.

There is a long initial latency period in the two high speed flows, during which time the growth rate is even slower than its asymptotic value. This may be due to the initial conditions. However, the normalized initial velocity perturbations were similar for all three cases represented on this figure, and this result may reflect a significant physical characteristic of developing shear layers. There has been no further investigation of this issue during the present work.

The asymptotic growth rates of these shear layer are given in Fig. 5. The growth rates are normalized by an incompressible rate which is obtained by assuming the $M_c = 0.2$ simulation to be essentially incompressible. There are few simulation data points, and the simulation at $M_c = 1.48$ had a strong density gradient across the layer. However, the trend observed in the simulations is clearly toward reduced turbulent mixing at high speeds.

Dominant Structure - There are significant differences in the vortex structures at low and high speeds. A side view of the spanwise vorticity for the $M_c = 0.2$ case is given in Fig. 6-a. The vorticity has largely coalesced into three principal "clumps." Figure 6-b gives a top view of pressure contours which identify low pressure regions on a few planes near the middle of the shear layer. The low pressure is associated with the vortex cores. The now classical picture of a flow dominated by spanwise vortices is evident, but a considerable amount of randomness in this structure is also present. Recall that this turbulence field is emerging from a purely random initial disturbance, and that the mean shear layer thickness has grown by a factor of ~ 4 only. The vorticity plot for this flow is not used to illustrate structure. The vorticity is sensitive to high wave number fluctuations which tend to be random, and this produces a very confusing plot. The pressure provides a form of integration over all fluctuations and gives a better picture of the large scale structure. The result demonstrates that the flow selects spanwise vortical structures.

The swept structures in the $M_c = 2.5$ case can be seen in the vorticity contour plots given in Fig. 7. The top view in Fig. 7-a gives the streamwise vorticity on several planes through the layer. The contour levels were selected to highlight the high-vorticity vortex cores. It was necessary to plot the vorticity on several planes because the vortices are also vertically inclined at a shallow angle. This vertical inclination is seen in a side view which shows the streamwise velocity in a single x-y plane. The top view indicates that the vortices are highly swept, at roughly $\beta = 77^\circ$ from the spanwise direction. An oblique view from above the layer, in Fig. 7-c, gives streamwise vorticity on z-y planes which are uniformly spaced in the streamwise direction. The highly swept vortices are again seen. Figure 8 gives a top view of the contours of the thermodynamic pressure. The contour levels are selected to highlight low pressure which is associated with the vortex cores seen in Fig. 7-a. The minimum contour level is 0.45 of the freestream pressure P_∞ , but the minimum pressure in the simulation was about $0.3 P_\infty$.

The majority of the pressure fluctuations in this simulation are closely related to the vortex structure. This may be of considerable importance because, as will be discussed below, the suppression of turbulence can be viewed as an effect of pressure-velocity correlations. If these pressure-velocity correlations depend on the vortex structure, then knowledge of the vortex structure will be required for statistical turbulence prediction methods.

As discussed in the section on boundary conditions, the structure of turbulence is constrained by assumption of spatial periodicity. The turbulence structure in the $M_c = 2.5$ simulation contains two fundamental periods in the spanwise and one in the streamwise. This simulation would force turbulence with a natural structure of for example, 1.5 or 2.5 periods in the spanwise direction onto the solution given in Fig. 7. Hence, the preferred sweep angle could be in the range -70° to -80° . This ambiguity does not alter the conclusion that highly swept vortices dominate the high speed mixing layer.

The effective convective Mach, which is the Mach number normal to the structures, is given by $M_{c,eff} = M_c \cos(\beta)$. At $M_c = 2.5$ and $\beta = 77^\circ$, $M_{c,eff} = 0.56$. This is clearly a subsonic Mach number, but transonic flow could be generated, depending on the nature of the structure. This simulation result is consistent with the theories presented above: The sweep angle is very large, even at this moderate Mach number, and of roughly the correct magnitude. At $M_{c,eff} = 0.56$, these turbulent structures exist just below the Mach number at which a (further) change in the angle of the structure is predicted by Eq. (32) and in Fig. 3.

The vortex structure in the high speed case is well defined and it exhibits considerably less randomness than in the low speed case. The sub-grid-scale viscous effects used in the simulations scales linearly with Mach number, which would provide a similar effective turbulent Reynolds number if the normalized turbulence were the same in both flows. The less vigorous normalized turbulence in the high speed case causes the effective turbulent Reynolds number to be lower, which restricts the range of scales of turbulence and makes it less chaotic. This is a deficiency which can easily be remedied, now that it is recognized. In the present results, it should principally affect the small turbulent scales, while the largest scales should be much less affected. The limited range of scales will affect the predicted levels of anisotropy because the small scales tend to be more isotropic, while the larger scales are less isotropic. Hence, the predicted levels of anisotropy may be artificially larger than in a high Reynolds number shear layer.

A very different turbulent structure was seen in two of the simulations. In the spatially and temporally evolving flows initialized with three modes selected from instability theory, the vortical structure was essentially spanwise. While the flow was at a lower convective Mach number, $M_c = 1.0$, it is in the range where the theory predicts a sweep angle of $\beta = 60^\circ$. The lack of sweep in this simulation suggests a strong dependence on the initial disturbance. It is possible that the flow is non-unique, a characteristic which could be exploited in flow control. However, this result clearly illustrates a potential hazard of initiating the flow with highly regulated disturbance modes.

With the above paragraph as a caveat on the veracity of the simulation results, it must further be noted that Papamoschou and Roshko⁸ have speculated that the dominant structures in their experiments were spanwise. Their argument was that structures were identified in optical records which integrated across the span of the layer, and that spanwise structures only would be preserved through the integration process. That speculation and the present findings are clearly in disagreement.

Shocklets - Two-dimensional simulations of compressible mixing layers have demonstrated the presence of shocklets which are associated with the passage of vortical structures. Transient shocks have also been observed in three-dimensional simulations of homogeneous turbulence. Furthermore, the existence of shocklets is central to some theories which attribute the reduced turbulent growth rates of high speed shear layers to the extra dissipation caused by these shocklets.

As the vortical structures become skewed, the effective Mach number decreases as $\cos(\beta)$. The vortex structure observed in the $M_c = 2.5$ case was swept so that $M_{c,eff} = 0.56$, and shocklets were, almost universally, not seen. At only one instant in time was a shock observed in the simulations of this and other high speed flows started with the random initial conditions. An effort was made to track that shock, but it disappeared very quickly.

The principal question would then seem to be: Under what conditions do shocklets constitute a significant phenomenon in turbulence? Shocklets were present in both spatially and temporally evolving simulations performed with the starting conditions prescribed from stability theory. Clearly, the simulations are capable of representing shocklets, and a flow with shocklets can evolve. Of the present results, those started from random initial conditions would seem to be more representative of a "natural" state of turbulence. However, this may not be so if the flow is prone to have a lengthy "memory" of the initial disturbances. Furthermore, certain types of additional strains such as lateral divergence ($\partial W / \partial z > 0$, in the present notation) would reduce the sweep angle of the vortices, literally, by stretching them into a more spanwise posture. This would increase their convective Mach number and the likelihood of shocklet formation.

One result of the present work is that shocklets are not required to reduce the growth rate of a shear layer at high convective Mach number. The significant growth rate suppression in the $M_c = 1.48$ and 2.5 cases was caused by a change in the dominant vortical structure, in the absence of shocklets.

$M_c = 4$ Case - A major goal of this work was to examine the results of simulations at as high a Mach number as possible. The $M_c = 2.5$ case falls in the high end of the supersonic range, but a case at $M_c = 4$ is into the realm of hypersonic flow. Calculations were performed using the same grid and procedure for generating the initial conditions as the $M_c = 2.5$ case. However, the initial disturbances decayed and the flow showed little tendency to generate a "turbulent" flow. Two more calculations of this case were performed, each with a reduced coefficient in the sub-grid-scale diffusion model, but this did not change the outcome.

The inability to generate a growing turbulent layer is most likely caused by some form of computational restriction imposed on the solution, but the implications for flow physics cannot be completely disregarded. It may be that the amplified structures are so highly inclined that they did not "fit" into the computational domain properly. Since the $M_c = 2.5$ case had only one structure in the streamwise direction and the ratio of streamwise/spanwise dimension is expected to increase with M_c , it is possible that a longer computational domain might be required to obtain a turbulent flow. (These possibilities were not recognized until the analysis was nearly completed, and there was insufficient time to attempt further simulations.)

It is unfortunate, but the failure to achieve a turbulent solution in this case, for reasons which may be due to limitations of the numerical simulations, does cast some doubt on the accuracy of the simulation at $M_c = 2.5$.

Turbulence Statistics - The statistics of these turbulent flows provide a completely different way to look at exactly the same physical phenomena. Statistics are important to consider because all mean flow calculations rely upon some form of statistical treatment of turbulence.

Turbulence statistics are obtained by averaging over the x- and z-directions, for which the turbulence is periodic, at one instant in time. The convergence of the statistics depends on the x-z area of the domain, and for these calculations the statistics are reasonably well,

but not completely, converged. That is, a simulation on a larger domain or a different realization of the same simulation would yield a slightly different answer. This is verified by noting that the normalized statistics are slightly different at different times, and that some statistics which should be exactly zero are slightly non-zero. However, the important trends that are identified in the data are unaffected by these small uncertainties.

In general, mass weighted or Favre' averaging is used, in which

$$u = U + u'', \quad U = \langle \rho u \rangle / \langle \rho \rangle \quad (33)$$

Conventional Reynolds averaging is also employed occasionally. Averages are denoted by $\langle \rangle$ brackets, although the "overbar" notation is also used elsewhere in this report (e.g., $\langle g \rangle = \overline{g}$).

In general the statistical results are normalized. Spatial dimensions are normalized by the shear layer thickness δ , for example, $\eta = y / \delta$. The edges are taken to be the points at which

$$U(y_{\text{edge}}) = U_{\text{min}} + 0.1 \Delta U \quad \text{and} \quad U(y_{\text{edge}}) = U_{\text{max}} - 0.1 \Delta U \quad (34)$$

The turbulent stresses and other higher order statistics are normalized by appropriate combinations of ΔU and the mean density, so that effects of the differing mean velocities is removed from the results.

In the following discussion, the results at $M_c = 0.2$ and $M_c = 2.5$ are contrasted. The low Mach number case is virtually incompressible, while the high speed case is very much affected by compressibility. The density ratio across both shear layers is unity.

The first data to consider are the mean momenta and density profiles, not normalized, given in Fig. 9. The low speed case exhibits a smooth hyperbolic tangent-like streamwise velocity profile, while ρ and ρV are roughly constant, as expected. The high speed case displays a streamwise velocity profile which has rather sharp corners, in contrast to the smooth profile at the lower Mach number. This difference in the velocity profiles is somewhat unexpected, and such pronounced sharp corners are not generally observed in a wide range experimental data. However, this trend is consistent some experimental measurements. The sharp corners on the velocity profile cause the maximum velocity gradient $\partial U / \partial y_{\text{max}}$ to be less than in a shear layer of similar total thickness, but at a low convective Mach number. This causes the vorticity thickness δ_ω , defined by $\Delta U = \delta_\omega (\partial U / \partial y)_{\text{max}}$ and normalized on its incompressible value, to be greater at higher M_c . It has been observed experimentally^{7,8} that the normalized growth rate for δ_ω is twice as large as the "visual" thickness or pitot thickness growth rate at high M_c . Hence, the trend toward a more nearly linear velocity profile is not inconsistent with experimental measurements.

The mean density is about 40% less than its freestream value near the center of the shear layer. At the center of the layer, turbulence accounts for a significant fraction of the total normal stresses, turbulence plus thermodynamic pressure. The turbulent $\langle \rho v'' v'' \rangle$ normal stress displaces some of the thermodynamic pressure and the density decreases with

the pressure. The instantaneous thermodynamic pressure in the cores of vortices in the shear layer is observed to be as low as $0.3 P_\infty$ in the $M_c = 2.5$ case.

The components of the normalized turbulent stress tensor $\langle \rho u_i' u_j' \rangle$ are given in Fig. 10. In the low speed case, the maximum normal stresses are in the range 0.03 to 0.04 and the maximum magnitude of the principal shear stress is about -0.02. These stresses are somewhat higher than typically observed in experiments.²⁰ The normal stresses are high by perhaps 20% to 40% while the shear stress is roughly 60% above the upper end of the experimental range. The cause of this discrepancy is unknown. It may be due to the effects of the limited range of scales in the simulation, a transitional effect, or the strength of the initial disturbance. This is an issue which deserves further scrutiny. The $\langle \rho u'' w'' \rangle$ and $\langle \rho v'' w'' \rangle$ shear stresses are close to zero, as they should be.

The stresses in the high speed case, given in Fig. 10, are very different than in the low speed layer. The maximum streamwise normal stress $\langle \rho u'' u'' \rangle$ is close to the value in the low speed case. However, the other normal stresses are approximately an order of magnitude less than in the low speed layer. Hence, there is a very unequal distribution of turbulence energy among the normal stresses, with the majority of the energy in the streamwise component. The shear stress is also significantly less than in the low speed case, which is of course necessary to be consistent with the reduced growth rate.

The accuracy of the normal stress results in the $M_c = 2.5$ case is a point of concern. This level of anisotropy is virtually unknown in any low speed turbulence. Only in transitional flows is turbulence essentially two-dimensional and, hence, highly anisotropic. As noted previously, the SGS transport does scale with the Mach number, which will cause the $M_c = 2.5$ case to be more laminar-like, and which may artificially increase the level of anisotropy. However, the global features of the $M_c = 2.5$ shear layer are consistent with theory and experiment. It is inappropriate to reject one result from this simulation while so many other aspects are reasonably accurate. Hence, the *trend* toward higher levels of anisotropy and high convective Mach numbers should be believed unless disproven.

One of the goals of this work is to determine the origins of the reduced shear stress, in terms of turbulent statistics. One possibility is that of a "purely compressible" mechanism. In a "purely compressible" mechanism the instantaneous density fluctuations due to fluid dynamic compression would correlate with velocity fluctuations in a manner that would reduce the shear stress. This possibility can be assessed by decomposing the full stress

$$\langle \rho u_i' u_j' \rangle \quad (35)$$

into its incompressible part

$$\langle \rho \rangle \langle u_i' u_j' \rangle \quad (36)$$

and a part which is purely due to compressibility effects, written for convenience as

$$\langle \rho u_i' u_j' \rangle - \langle \rho \rangle \langle u_i' u_j' \rangle \quad (37)$$

If there is a high correlation between the blobs of fluid which carry the fluctuating second moment of velocity $u_i' u_j'$ and the perturbation density, then the purely compressible part,

Eq. (37), will be significant. Figure 11 gives this decomposition for $\langle \rho u''u'' \rangle$ and $\langle \rho u''v'' \rangle$. In the $M_c = 0.2$ case, the compressible part is negligible, as expected. At $M_c = 2.5$ the compressible part is not zero, but it is roughly an order of magnitude less than the total stress. The decomposition for the shear stress $\langle \rho u''v'' \rangle$ at $M_c = 2.5$ also shows the compressible part to be small. The compressible part generally has the opposite sign of the stress itself, and hence contributes to a reduction in the stress. For this case in which there is no density stratification, the total stresses $\langle \rho u_i''u_j'' \rangle$ are not very different from the incompressible part of the stresses $\langle \rho \rangle \langle u_i''u_j'' \rangle$. This result suggests that purely compressible mechanisms which depend upon significant correlations between the instantaneous velocity fluctuations, $u_i''u_j''$, and the perturbation density may not be very important.

Anisotropy of the normal stresses is, however, very important. The principal source of the shear stress is its production term,

$$P_{uv} = -\langle \rho v''v'' \rangle \partial U / \partial y \quad (38)$$

for this simple shear layer. The reduced normal stress $\langle \rho v''v'' \rangle$ almost guarantees that shear stress will be small as well, unless drastic reductions in the mechanism which destroy $\langle \rho u''v'' \rangle$ also occur. Hence, the origins of the anisotropic normal stresses may be, from the statistical point of view, an important contributor to compressibility effects.

Pressure-Velocity Terms - Anisotropy is regulated by fluctuating pressure-velocity interactions. In simple shear flows, the turbulence energy is formed as streamwise fluctuations. This energy is then distributed to the other energy components by the pressure-velocity interactions. It is the velocity-pressure gradient term which appears naturally in the Reynolds-stress transport equations. This will be denoted herein as

$$\phi_{ij} = -\langle u_i'' \partial p' / \partial x_j \rangle - \langle u_j'' \partial p' / \partial x_i \rangle \quad (39)$$

This term includes both the pressure-strain and pressure-diffusion terms. Figure 12 gives the velocity-pressure gradient term for all six stresses in the $M_c = 0.2$ and $M_c = 2.5$ cases. Because of the minus sign in Eq. (36), a positive value in Fig. 12 acts to reduce positive stress or increase a negative stress. (For consistency of notation, let $\phi_{12} \equiv \phi_{uv}$, etc.)

The ϕ_{uu} terms are rather similar in the high and low speed results; both reduce $\langle \rho u''u'' \rangle$, although ϕ_{uu} is slightly larger for the low speed case. Recall from Fig. 10 that $\langle \rho u''u'' \rangle$ is also similar in the low and high speed flows. The ϕ_{uv} terms are also comparable, but now this term is slightly larger in the high speed case. However, there is an enormous "hidden" difference: the shear stress and its production in the high speed case is only a small fraction of the shear stress in the low speed case. That is, the ratios $-\phi_{uv} / \langle \rho u''v'' \rangle$ and $-\phi_{uv} / P_{uv}$ increase significantly as the convective Mach number rises. The "common wisdom" in turbulence research is that the rate at which the shear stress is reduced by pressure-velocity interactions is proportional to the magnitude of the shear stress and its production P_{uv} ; this is clearly not satisfied across the range of convective Mach numbers considered here.

Another large difference is seen in ϕ_{vv} . This term is responsible in part for energy transfer from $\langle \rho u''u'' \rangle$ to $\langle \rho v''v'' \rangle$. The rate of creation of $\langle \rho v''v'' \rangle$ by ϕ_{vv} in the high speed layer is only half of that rate in the low speed layer. To reiterate, energy is extracted from

the mean flow as $\langle \rho u''u'' \rangle$ and then converted to $\langle \rho v''v'' \rangle$ by ϕ_{uu} and ϕ_{vv} ; $\langle \rho v''v'' \rangle$ is required to generate $\langle \rho u''v'' \rangle$ via P_{uv} and, hence, is critical to the turbulent shear stress. The reduced transfer from $\langle \rho u''u'' \rangle$ to $\langle \rho v''v'' \rangle$ disrupts a chain of events which normally produces the shear stress.

Are these statistical results consistent with the swept vortical structures of turbulence? A vortex strongly couples the fluctuating velocity components normal to its axis. A spanwise (z-oriented) vortex must have roughly equal magnitudes of u' and v' irrespective of w' , and a streamwise (x-oriented) vortex has roughly equal magnitudes of v' and w' regardless of u' . This is consistent with the turbulent normal stresses $\langle \rho v''v'' \rangle$ and $\langle \rho w''w'' \rangle$ in Figure 10 which are roughly equal. Streamwise fluctuations u' exist in this flow without being strongly coupled to v' and w' . The source of turbulence energy in these flows is the production term for the streamwise fluctuations

$$P_{uu} = - \langle \rho u''v'' \rangle \partial U / \partial y \quad (40)$$

The streamwise structures are unable to couple this source of turbulence energy to the vertical fluctuations $\langle \rho v''v'' \rangle$ which are required to generate shear stress. Hence, these statistical details of turbulence are consistent with the vortex structure. However, the increased suppression of $\langle \rho u''v'' \rangle$ by ϕ_{uv} cannot, at present, be linked to the vortical structure.

The following seem to be significant findings from the analysis of simulation data at $M_c = 0.2$ and $M_c = 2.5$.

1. In the $M_c = 2.5$ case, the velocity profile exhibits a sharp transition at the edge of the layer, which is very unlike the smooth hyperbolic tangent-like profile in the low speed case.
2. The turbulent normal stresses are very anisotropic at $M_c = 2.5$, with the streamwise component $\langle \rho u''u'' \rangle$ much larger than $\langle \rho v''v'' \rangle$ and $\langle \rho w''w'' \rangle$. The low speed turbulence is more nearly isotropic.
3. The difference between the full stresses $\langle \rho u_i''u_j'' \rangle$ and its incompressible part $\langle \rho \rangle \langle u_i''u_j'' \rangle$ is small when there is no density stratification.
4. The gross compressibility effect, that of reducing the growth shear stress, may be explained by the pressure-velocity correlations which suppress the shear stress and which do not rapidly generate $\langle \rho v''v'' \rangle$ from the turbulence energy in $\langle \rho u''u'' \rangle$. Again, $\langle \rho v''v'' \rangle$ is required for generation of the shear stress by the production term P_{uv} .
5. The swept vortex idealization of high speed turbulence is consistent with these statistical results.

The statistical analysis is incomplete. The velocity-pressure gradient terms should be decomposed into the pressure-strain and pressure-diffusion terms to gain further insight, and then the pressure strain term should be further broken into the so-called return-to-isotropy and rapid components, if possible. It may also be important to determine what

portion of the reduction in shear stress at high Mach number can be attributed to specific statistical mechanisms, and to assess the possible link between the pressure-velocity statistics and the swept vortex structure.

The Role of Dissipation - Proposals have been put forth (e.g., Zeman²¹) concerning the role of the dissipation rate in compressible turbulence. The argument is that dissipation rate ϵ is increased due to shocklets or dilatation which reduces the turbulence energy k and the length scale $L \sim k^{3/2}/\epsilon$. The present results do not support these proposals.

Firstly, shocklets are virtually non-existent in the present simulation. Secondly, the present simulations predict the reduced spreading rate even though they cannot accurately predict details of dissipation phenomena. The sub-grid-scale viscous model on which dissipation depends is an eddy-viscosity model with poor accuracy, and the accuracy of the differencing scheme becomes increasingly poor at the high wave numbers at which dissipation is important. Hence, the accuracy for dissipation is poor. The fact that these simulations predict the decreased mixing at high M_c despite the poor accuracy for dissipative phenomena strongly suggests that dissipation is not the principal cause of the reduced shear stress in high Mach number turbulence.

Limitations - Before closing, it is worth reiterating the primary assumptions which may compromise the accuracy of the simulation results. In most cases these issues are not imposed by the available simulation technology, but rather by the limited scope of a Phase I effort.

1. Most simulations are of a temporally evolving shear layer in which the assumption of spatial periodicity is made. Streamwise gradients in the shear layer thickness, entropy, and the evolution of the dominant structure, which are disregarded, may contribute to errors in the results. In the one comparison between similar flows that were computed both as spatially and temporally evolving, the dominant structures were very similar. Hence, this is not felt to be a major concern.
2. The periodic boundary conditions require an integer number of the dominant vortex structures to fit into the computational domain. This means that there is some uncertainty in the nature of these structures, which depends on the size of the computational domain. For the $M_c = 2.5$ case this ambiguity is small, $\pm 5^\circ$ in sweep angle, and does not materially affect the conclusions of this study. However, there may have been a significant effect in the case of the $M_c = 4$ simulation.
3. All simulations have been started with prescribed initial conditions, and the dependence on these initial conditions is large. It has been assumed that the random initial conditions give the most "natural" well-developed turbulence, but this is not proven.
4. These are, in effect, low Reynolds-number simulations because of the limited range of scales which are resolved. While the $M_c = 0.2$ solution contained a chaotic-looking fine scale imposed upon the dominant vortical structures, the $M_c = 2.5$ case was more nearly dominated by the large scale structure. This

problem may have biased some results, especially those concerning the level of anisotropy. The present study should be recognized as a limited investigation of the changes in turbulence due to convective Mach number because of the restricted range of scales.

5. The sub-grid-scale stresses are treated with a very simple model which undoubtedly has poor accuracy. Hence, the small scale phenomena related to dissipation will be represented inaccurately.

These limitations should affect, in general, details in the simulation results, not the major conclusions. Only the issue regarding the form of the initial disturbance can have a significant effect on the basic findings regarding the changes in turbulence as the convective Mach number becomes large.

SUMMARY AND CONCLUSIONS

The objective of the present work has been to identify major changes in turbulence as the Mach number becomes very large. The present effort is of limited scope and has focused on turbulence in an ideal gas, although it is recognized that many factors other such as wall catalysis, real gas and rarefied gas effects can be very significant in hypersonic flows. The present work has involved theoretical analyses and large eddy simulations of plane free shear layers.

The present results provide broad support for the idea that the dominant vortical structures of turbulence become swept in a streamwise direction at high convective Mach numbers. One analysis is widely applicable to two-dimensional shear flows in the limit of the Mach number tending to infinity. It indicates that entropy constraints restrict vortices to be in the streamwise direction, which minimizes entropy production. Based on this finding, a simple swept vortex model for planar free shear layers was constructed. This model makes predictions about the sweep angle of the dominant vortices and about the layer's growth rate over the full Mach number range. The growth rate predictions are consistent with experimental results, and the sweep angle predictions are generally in agreement with simulation results. This model also predicts that the sweep angle is large enough for the flow normal to the vortices to remain subsonic. Hence, shocks will generally be avoided in plane free shear flow.

The concept behind the simple vortex model, that it is the effective velocity normal to the vortical structures that determines the shear layer's growth, is not unique to the present effort. However, the present theory has been used to make predictions about vortex sweep angles and growth rates, which are confirmed in numerical simulations of the full nonlinear vortex development.

The underlying mechanism by which high speed turbulence avoids shocks is not clearly known. The present result suggests that it may be a straightforward compressibility effect, like the one which effects compressible subsonic spanwise vortices. Other theories have entertained the possibility that nascent shocks cause spanwise vortices to bifurcate and sweep. The predictions these theories make about the shear layer growth and sweep angle are not very different. However, the underlying physics are different, and these differences may become critical in future modeling efforts or in flows other than the plane shear layer.

Simulations at convective Mach numbers of $M_c = 0.2, 1.48$ and 2.5 were evaluated. The dependence of the shear layer's growth rate upon Mach number is in general agreement with experiment and the vortex model theory. The structures which dominate these shear layers are spanwise at $M_c = 0.2$ and swept about 75° toward the streamwise direction for the high speed flows. The effective convective Mach number, normal to the structure, is approximately $M_{c,eff} \sim 0.6$, which is subcritical.

Shock waves were not observed in these randomly initiated simulations, except on one very brief occasion. The absence of shocks is incompatible with theories which rely on additional shock-related dissipation to account for the reduced mixing in high speed turbulence.

Significant dependence of the simulation results upon the perturbations used to initiate the calculations was observed. The flows generated by random forcing are believed to be representative of "natural" turbulence-initiating disturbances. Simulations initiated with specific perturbation modes selected from stability calculations contained structures which were spanwise and which contained strong shocks. These results are probably anomalous. However, some aircraft may preferentially excite specific modes, and this result may have important implications. This result clearly indicates that the starting conditions for simulations must be treated carefully.

A statistical analysis of the simulation results was performed, and there are several significant differences between the $M_c = 0.2$ and 2.5 cases. It can be argued that the more important among these are related to the change of sweep angle of the dominant vortical structures. For example, the highly swept structures cannot rapidly transfer energy of streamwise fluctuations into normal and spanwise fluctuations; this disrupts a critical chain of events that generates shear stress (in low speed flows).

FUTURE WORK

There are at least three areas on which future work should focus. The first is the resolution of certain issues raised in this Phase I study. Some aspects of the present work were based on unproven assumptions or were compromised slightly by the need for expediency. Now that these issues are reasonably well defined, they can be resolved. One significant issue is that the underlying cause of vortex sweep is not known. It should be possible to construct careful simulation tests to identify the cause of this phenomenon.

A second aspect of any future work is the consideration of more complex flows. Turbulent flows that are wall-bounded, affected by mean streamwise vorticity, three-dimensional in the mean, separating, and affected by shock interactions, for example, are of great importance to high speed aircraft. Real gas and rarefied gas effects are also important. The results of the present study may suggest trends, but they cannot be extrapolated to these other flow phenomena. The Mach number dependent structural changes seen in the plane shear layer may or may not be widely significant in other flows. Even simple phenomena such as lateral divergence ($\partial W / \partial z < 0$, in the present notation) may significantly affect the characteristics of turbulence. A few classes of flows, which embody critical aspects of high speed turbulence or which are deemed to be most important technologically, would be studied.

A third area of importance is to provide for improved flow prediction methods. Work in the first two areas will generate understanding of the underlying flow physics, but quite often there is a huge gap between that knowledge and the statistical models required for prediction methods. One critical aspect of this work would be to identify the relationship between turbulence statistics and the dominant structure of turbulence, assuming such a link exists. The analyses performed in the present study should provide a foundation for developing this relationship. The present work suggests that the vortical structure plays a role in the statistical phenomena which must be modeled in existing advanced models. If so, then some means of solving equations for the structural characteristics, or of inferring structure from the computed turbulence quantities, must be developed. The logical conclusion to this line of thinking could be that a new class of turbulence models is required.

REFERENCES

1. Bradshaw, P., editor: Turbulence. Topics in Applied Physics, Vol. 12, Springer-Verlag, 1972.
2. Hesselink, L.: Digital Image Processing in Flow Visualization. Annual Review of Fluid Mechanics, Vol. 20, 1988, p. 421.
3. Rogallo, R. S. and Moin, P.: Numerical Simulation of Turbulent Flows. Annual Review of Fluid Mechanics, Vol. 16, 1984, p. 120.
4. Morkovin, M. V.: The Effects of Compressibility on Turbulent Flows. In The Mechanics of Turbulence, A. Forre, editor, (Gordon and Breach), 1964.
5. Harvey, J., Bergman, R. C., and Holden, M. S.: An Experimental Study of Hypersonic Turbulence on a Sharp Cone. AIAA Paper 89-1866.
6. Mikulla, V. and Horstman, C. C.: Turbulence Measurements in Hypersonic Shock-Wave Boundary-Layer Interaction Flows. AIAA Journal, Vol. 14, May 1976, p. 568-575, also AIAA Paper 76-0162.
7. Bodganoff, D. W.: Compressibility Effects in Turbulent Shear Layers. AIAA Journal, Vol. 21, No. 6, 1983, p. 926.
8. Papamoschou, D. and Roshko, A.: The Compressible Turbulent Shear Layer: An Experimental Study. Journal of Fluid Mechanics, Vol. 197, 1988, p. 453.
9. Lele, S.: Direct Numerical Simulation of Compressible Free Shear Flows. AIAA 89-0374, 1989.
10. Nixon, D., Keefe, L. R., and Kuhn G. D.: The Effects of Compressibility on a Supersonic Mixing Layer. AIAA Paper 90-0706, 1990.
11. Laderman, A. J. and Demetriades, A.: Mean and Fluctuating Flow Measurements in the Hypersonic Boundary Layer Over a Cooled Wall. Journal of Fluid Mechanics, Vol. 63, Pt. 1, 1974.
12. Seiner, J. M., "Advances in High Speed Aeroacoustics," AIAA-84-2275.
13. Thompson, K. W., "Time Dependent Boundary Conditions for Hyperbolic Systems," J. Comp Phys., Vol. 68, No. 1, Jan. 1987, pp. 1-24.
14. Childs, R. E., Bower, W., and Chimielewski, G.: Jet Noise Predictions Using Navier-Stokes Simulations. AIAA Paper 91-0493, 1991, see also the Task 2 Report on Contract NAS1-18745.
15. Rodman, L. C.: Meteorological Model Analysis for Numerical Weather Prediction, presented at 9th Americal Meteorological Society Conference on Numerical Weather Prediction, Denver, CO, oct. 1991.
16. Childs, R. E., Nixon, D., Kuhn, G. D., and Perkins, S. C., Jr.: Further Studies of Impinging Jet Phenomena. AIAA-87-0017.
17. Childs, R. E. and Nixon, D.: Turbulence and Fluid/Acoustic Interaction in Impinging Jets. SAE Paper No. 872345, presented at the International Powered Lift Conference, Santa Clara, CA, Dec. 7-10, 1987.
18. Sandham, N. D., and Reynolds, W. C.: The Compressible Mixing Layer: Linear Theory and Direct Simulation, AIAA-89-0371.
19. Wygnanski, I. and Fiedler, H. E.: The Two-Dimensional Mixing Layer, Journal of Fluid Mechanics, Vol. 41, part 2, pp. 327-361, 1970.
20. Zeman, O.: Dilatation Dissipation: The Concept and Application in Modeling Compressible Mixing Layers, Physics of Fluids A, Vol. 2, No. 2, 1990, pp.178-188.

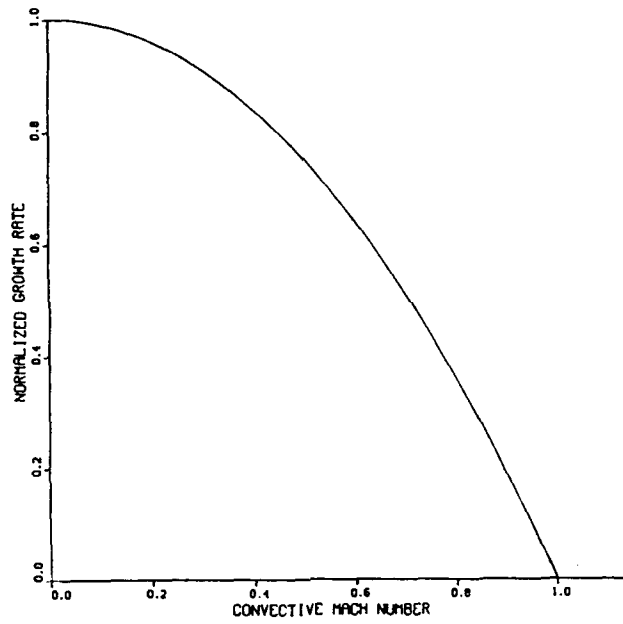


Figure 1. Assumed mixing layer growth rate versus convective Mach number for two-dimensional vortex structures, $\sigma_{2D}(M_c)$.

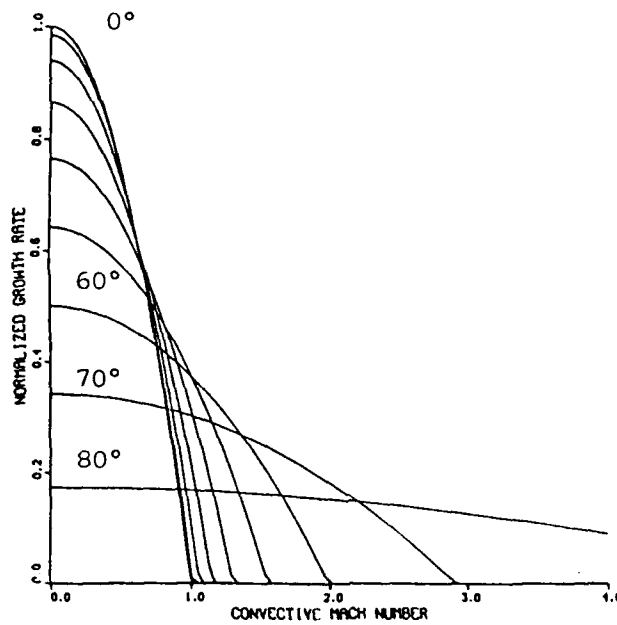


Figure 2. Predicted growth rate of shear layer with sweep permitted, $\sigma_{3D}(M_c, \beta)$.

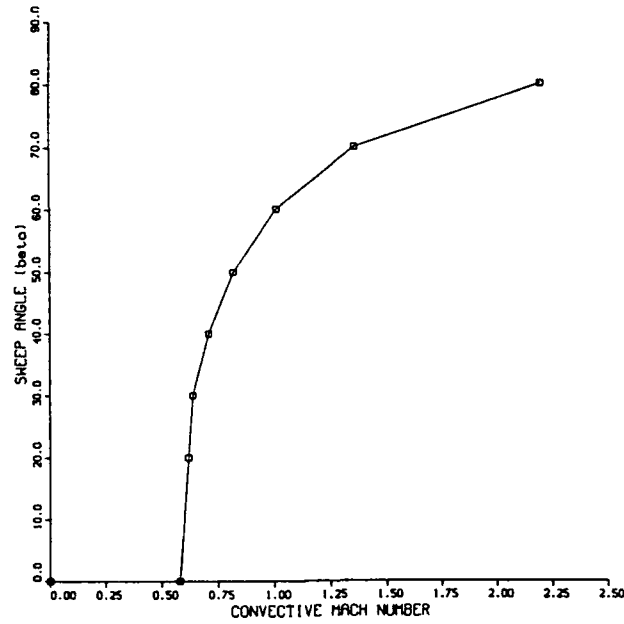


Figure 3. Sweep angle for maximum growth, $\beta_{\sigma, \max}(M_c)$.

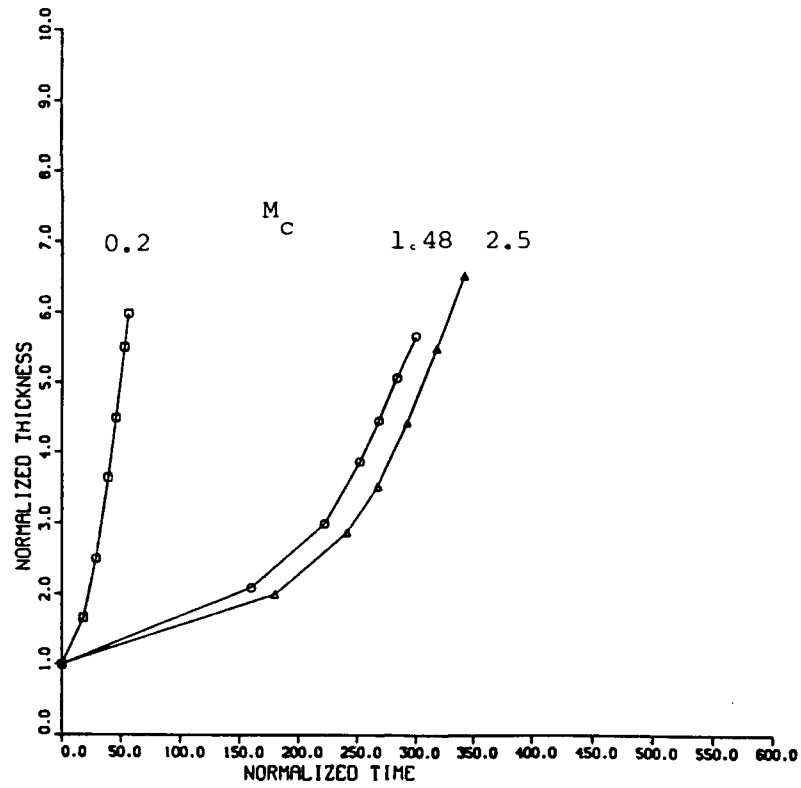


Figure 4. Temporal growth of shear layer thickness δ/δ_0 as function of non-dimensional time tU/δ_0 , from simulations.

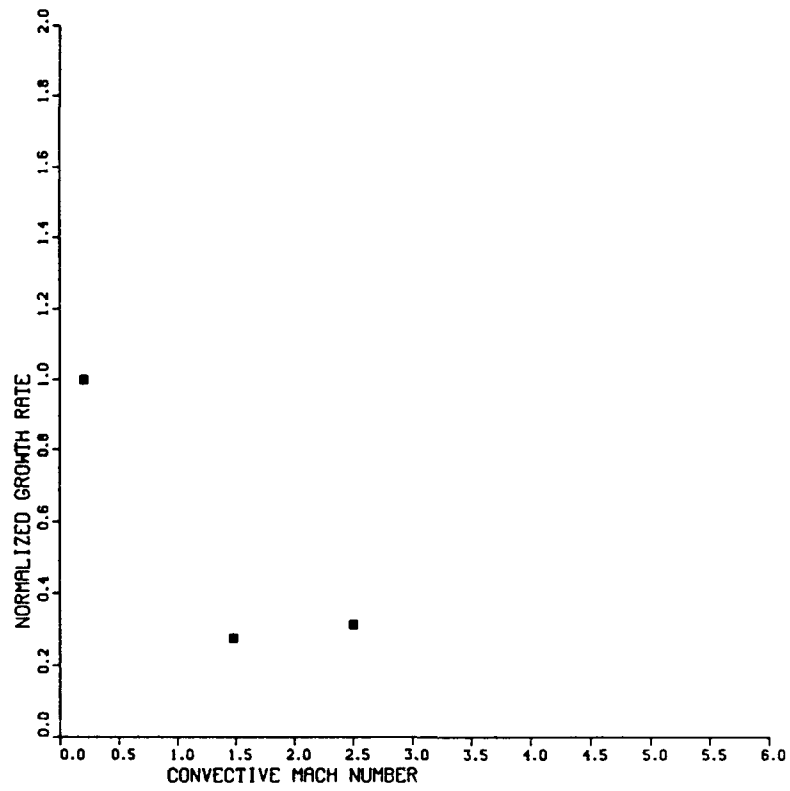


Figure 5. Equivalent asymptotic shear layer growth rate $d\delta/dx$, from simulations, normalized by $d\delta/dx$ at $M_c = 0.2$.

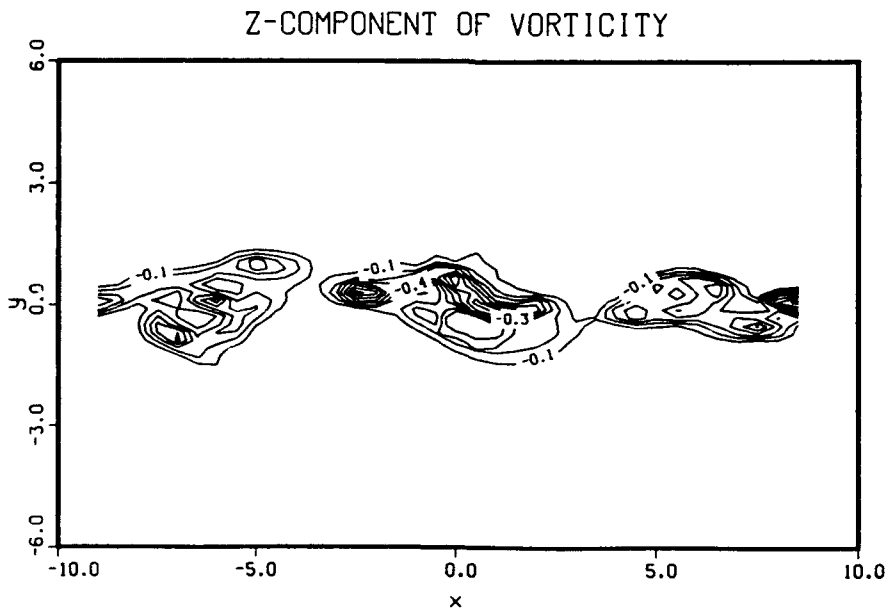


Figure 6(a). Contours of side view of instantaneous spanwise vorticity.

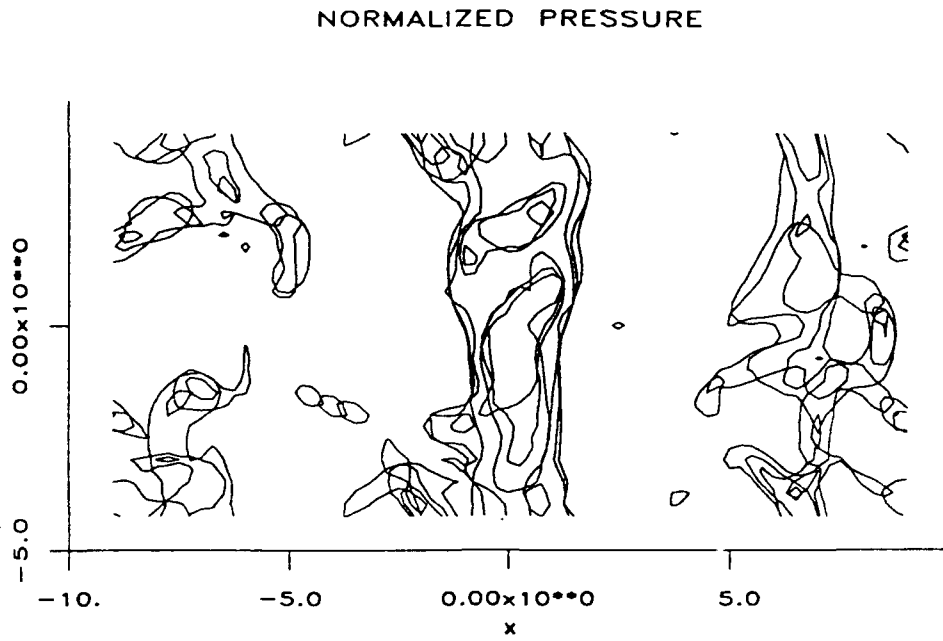


Figure 6(b). Contours of top view of low pressure associated with vortex cores, for $M_c = 0.2$ case.

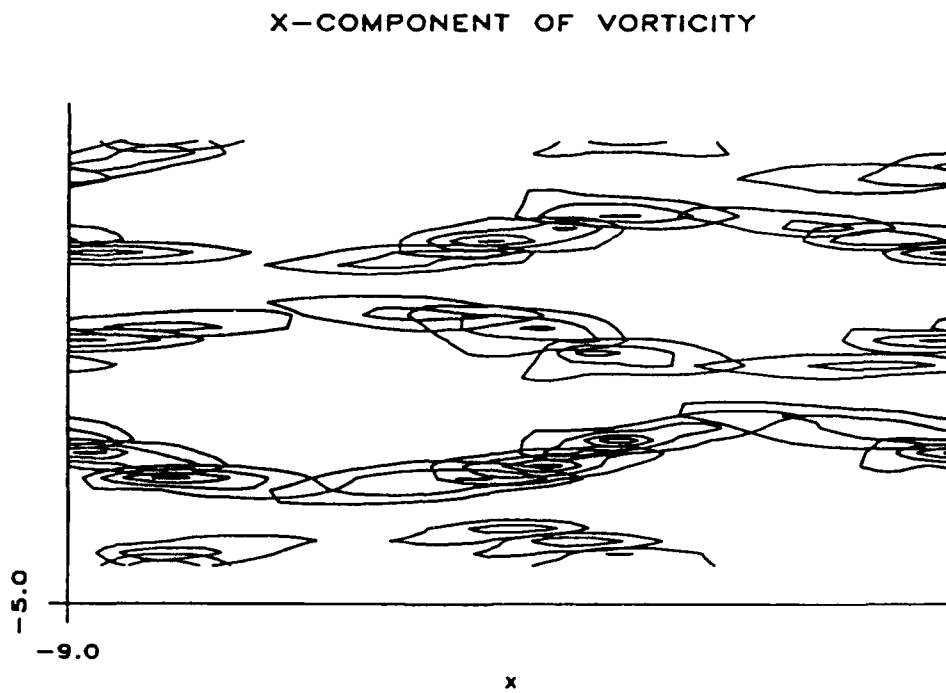


Figure 7(a). Contour plots for $M_c = 2.5$ case; top view of streamwise vorticity from above shear layer.

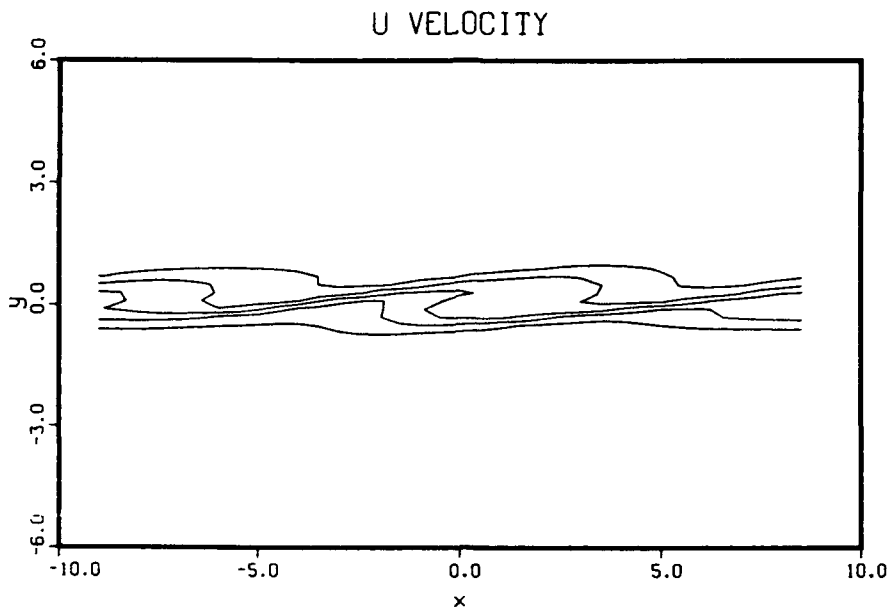


Figure 7(b). Contour plots for $M_c = 2.5$ case; side view of streamwise velocity, showing streamwise inclination,

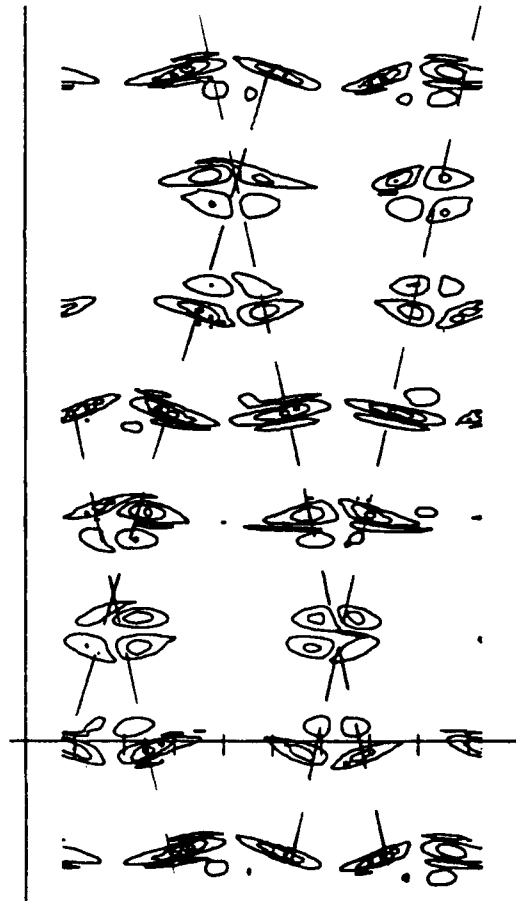


Figure 7(c). Contour plots for $M_c = 2.5$ case; oblique view of streamwise vorticity from above shear layer.

NORMALIZED PRESSURE

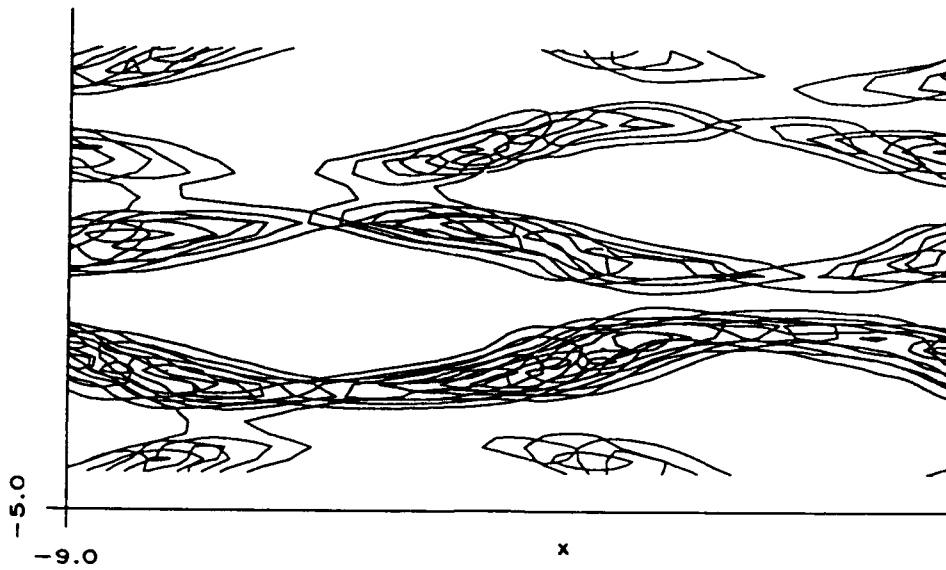


Figure 8. Contours of instantaneous low pressure associated with vortex cores for $M_c = 2.5$ case; top view as in Fig. 7-a.

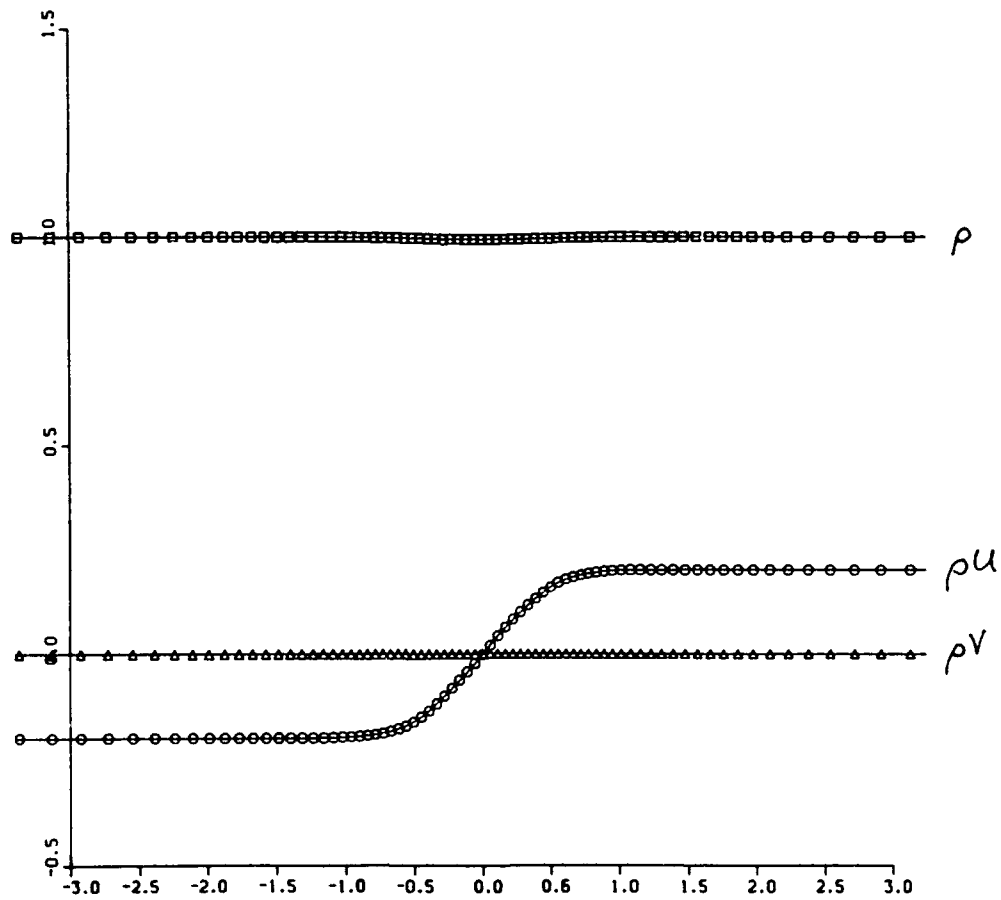


Figure 9(a). Mean density and momenta for $M_c = 0.2$ plotted versus normalized coordinate $\eta = y/\delta$.

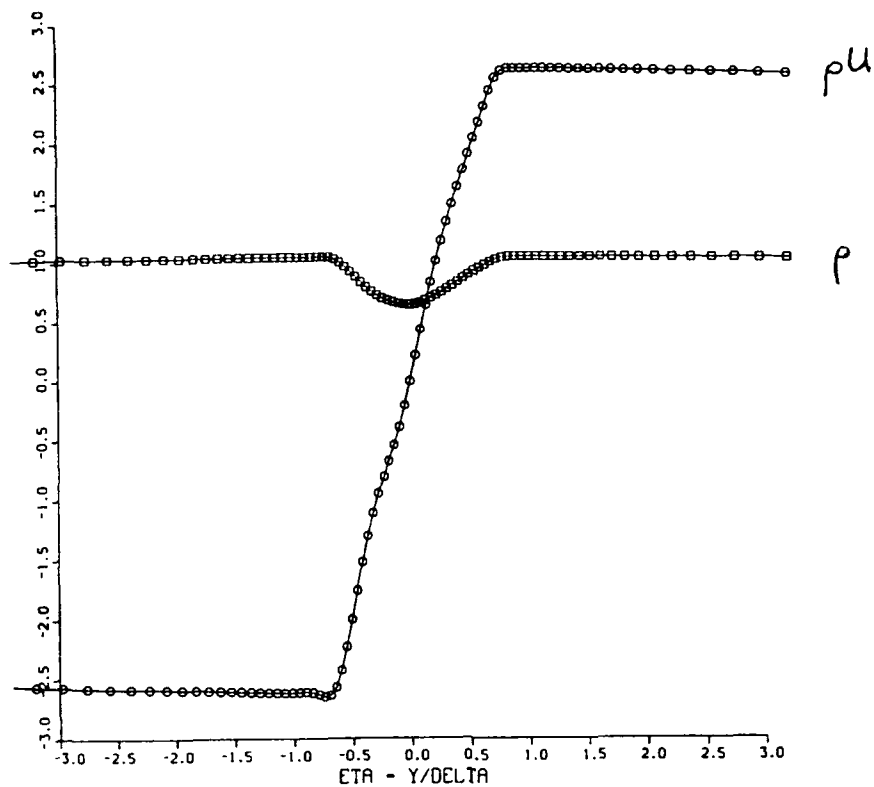


Figure 9(b). Mean density and momenta for $M_c = 2.5$ cases, plotted versus normalized coordinate $\eta = y/\delta$.

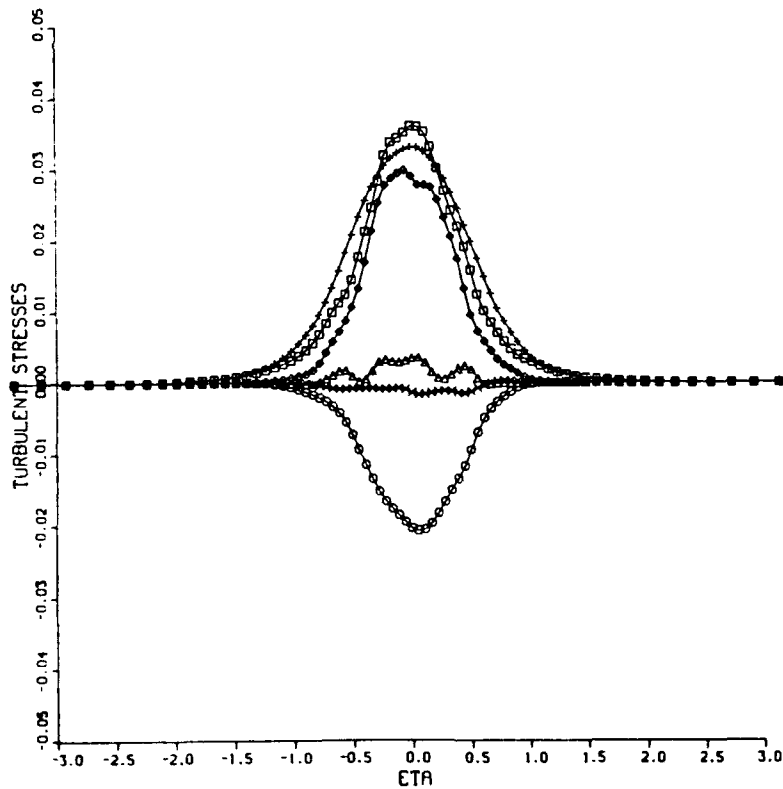


Figure 10(a). Turbulent stresses $\langle \rho u_i' u_j' \rangle$ for $M_c = 0.2$ case. (Notation is $\square = \langle \rho u'' u'' \rangle$; $+$ = $\langle \rho v'' v'' \rangle$; $\diamond = \langle \rho w'' w'' \rangle$; $\circ = \langle \rho u'' v'' \rangle$; $\Delta = \langle \rho u'' w'' \rangle$; $\times = \langle \rho v'' w'' \rangle$.)

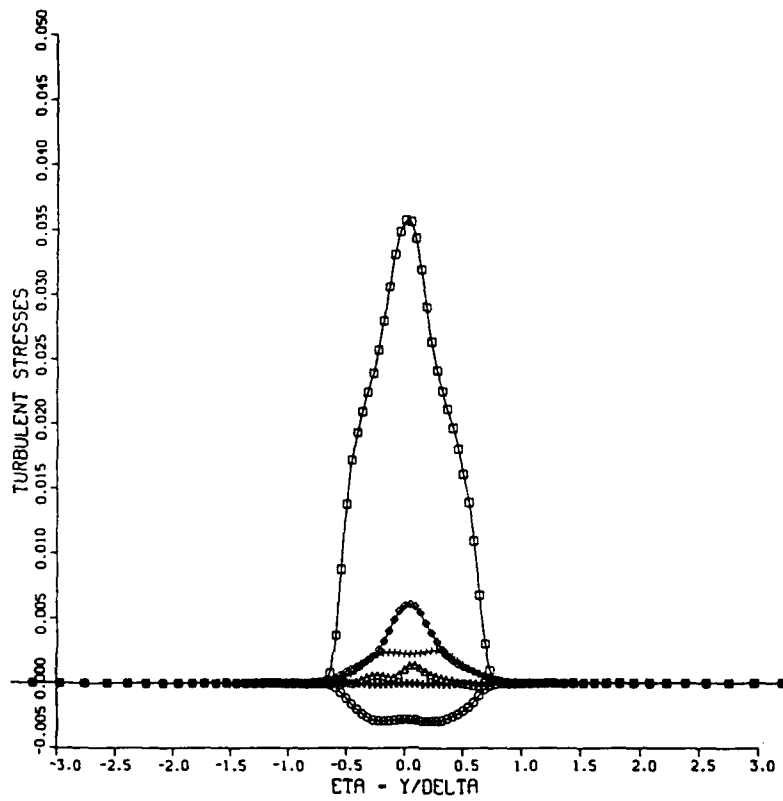


Figure 10(b). Turbulent stresses $\langle \rho u_i'' u_j'' \rangle$ for 2.5 case. (Notation is $\square = \langle \rho u'' u'' \rangle$; $+$ = $\langle \rho v'' v'' \rangle$; $\diamond = \langle \rho w'' w'' \rangle$; $o = \langle \rho u'' v'' \rangle$; $\Delta = \langle \rho u'' w'' \rangle$; $x = \langle \rho v'' w'' \rangle$.)

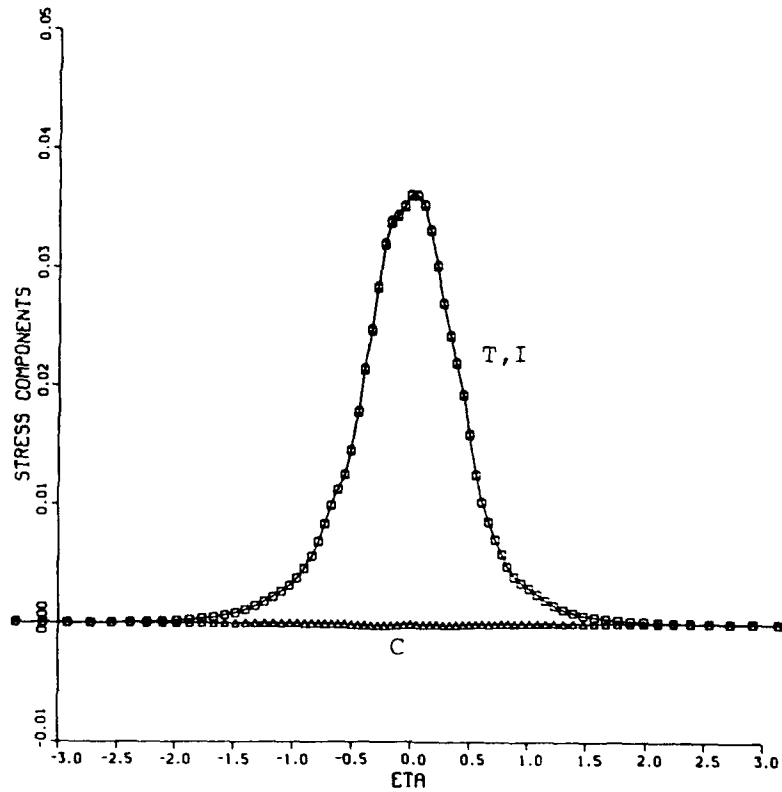


Figure 11(a). Decomposition of the total turbulent stresses (T) into incompressible (I) and purely compressible (C) parts, defined by Eq. 36 and 37, for $\langle \rho u'' u'' \rangle$ at $M_c = 0.2$.

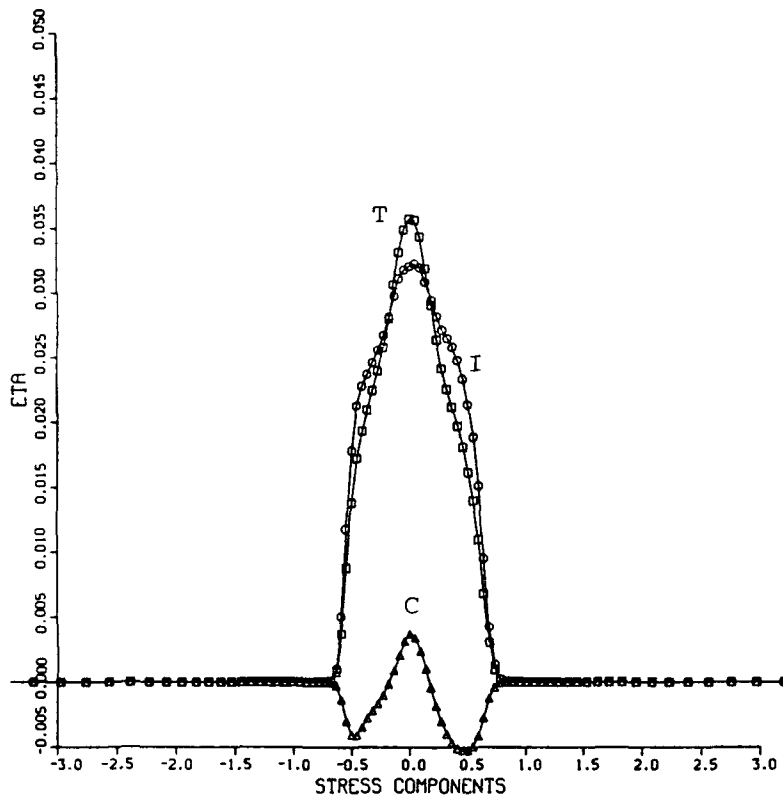


Figure 11(b). Decomposition of the total turbulent stresses (T) into incompressible (I) and purely compressible (C) parts, defined by Eq. 36 and 37, for $\langle \rho u''u'' \rangle$ at $M_c = 2.5$.

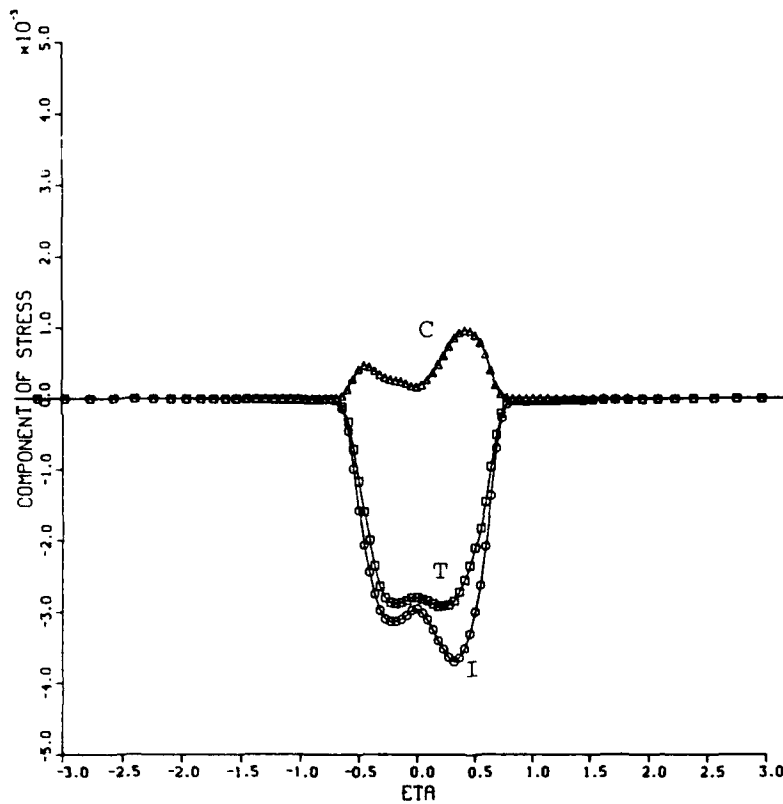


Figure 11(c). Decomposition of the total turbulent stresses (T) into incompressible (I) and purely compressible (C) parts, defined by Eq. 36 and 37, for $\langle \rho v''v'' \rangle$ at $M_c = 2.5$.

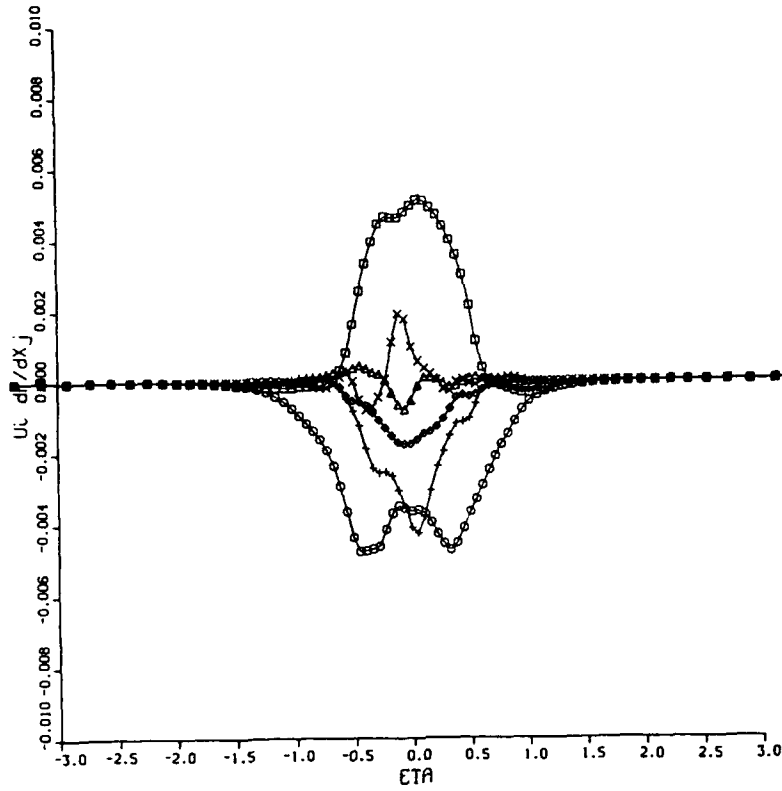


Figure 12(a). Velocity-pressure gradient terms, ϕ_{ij} defined in Eq. (39) for $M_c = 0.2$ case. (Symbols as in Fig. 10)

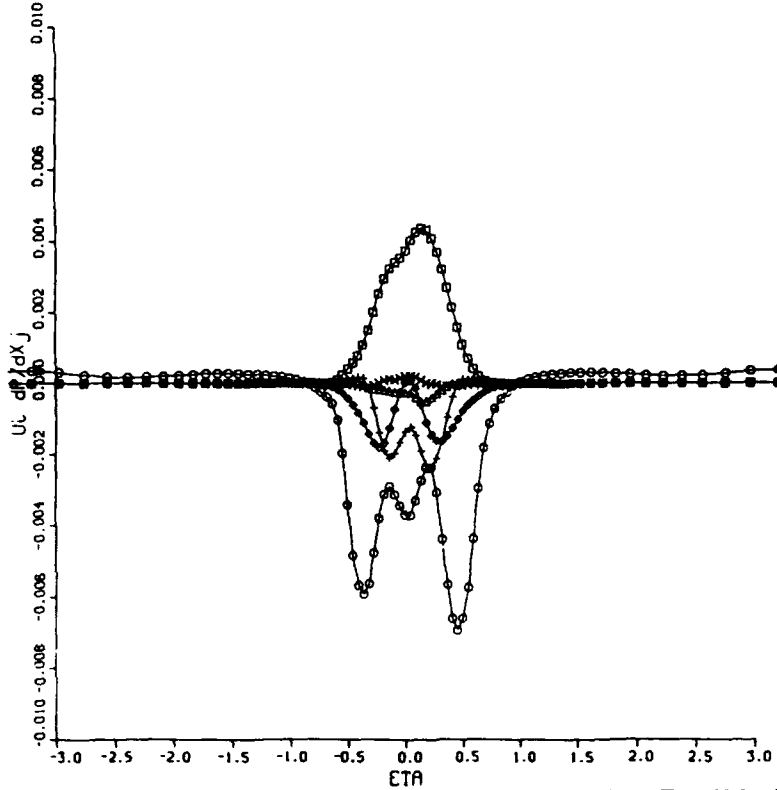


Figure 12(b). Velocity-pressure gradient terms, ϕ_{ij} defined in Eq. (39) for $M_c = 2.5$ case. (Symbols as in Fig. 10)